

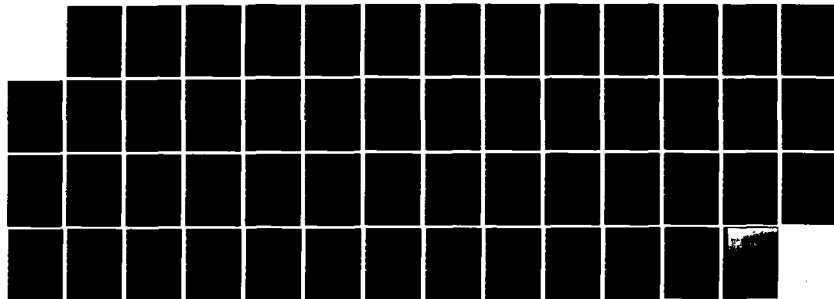
AD-A132 794

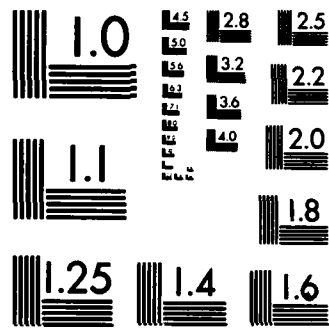
INVERSION OF THE ACOUSTIC PLANE WAVE REFLECTION
RESPONSE OF A LAYERED OCE. (U) DEFENCE RESEARCH
ESTABLISHMENT PACIFIC VICTORIA (BRITISH COLU.

1/1

UNCLASSIFIED

D J THOMSON ET AL. 04 AUG 83 DREP-TR-83-1 F/G 20/1 NL





MICROCOPY RESOLUTION TEST CHART
NATIONAL BUREAU OF STANDARDS-1963-A



AD-A132794

Inversion of the Acoustic Plane Wave Reflection Response of a Layered Ocean Bottom

D. J. Thomson
R. K. Chow
Defence Research Establishment Pacific

4 August 1983

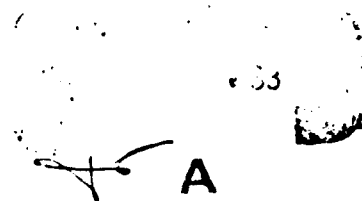
DTIC FILE COPY



Defence Research Establishment Pacific
Victoria, B.C. V0S 1B0, Canada



Naval Underwater Systems Center
Newport, Rhode Island • New London, Connecticut



Approved for public release; distribution unlimited.

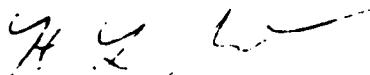
83 09 22 158

Preface

The work in this report was started by Drs. D. J. Thomson and R. K. Chow at the Defence Research Establishment Pacific, Victoria, British Columbia. The effort was continued and completed while Dr. Thomson was a Canadian exchange scientist at the Naval Underwater Systems Center, New London, Connecticut.

The Technical Reviewer for this report was Roy Deavenport (Code 3342).

APPROVED: 4 August 1983



**Dr. H. L. Grant
Chief Defence Research
Establishment Pacific**

APPROVED: 4 August 1983



**Earle L. Messere
Technical Director
Naval Underwater Systems Center**

**Inquiries concerning this report
should be directed to Code 33, New London
Laboratory, Naval Underwater Systems Center,
New London, Connecticut 06320**

REPORT DOCUMENTATION PAGE		READ INSTRUCTIONS BEFORE COMPLETING FORM								
1. REPORT NUMBER TR 6925	2. GOVT ACCESSION NO. AD-A132794	3. RECIPIENT'S CATALOG NUMBER								
4. TITLE (and Subtitle) INVERSION OF THE ACOUSTIC PLANE WAVE REFLECTION RESPONSE OF A LAYERED OCEAN BOTTOM		5. TYPE OF REPORT & PERIOD COVERED								
		6. PERFORMING ORG. REPORT NUMBER								
7. AUTHOR(s) D. J. Thomson R. K. Chow		8. CONTRACT OR GRANT NUMBER(s)								
9. PERFORMING ORGANIZATION NAME AND ADDRESS Naval Underwater Systems Center New London Laboratory New London, CT 06320		10. PROGRAM ELEMENT, PROJECT, TASK AREA & WORK UNIT NUMBERS 633K15								
11. CONTROLLING OFFICE NAME AND ADDRESS Naval Underwater Systems Center New London Laboratory New London, CT 06320		12. REPORT DATE 4 August 1983								
		13. NUMBER OF PAGES 49								
14. MONITORING AGENCY NAME & ADDRESS (if different from Controlling Office)		15. SECURITY CLASS. (of this report) UNCLASSIFIED								
		15a. DECLASSIFICATION/DOWNGRADING SCHEDULE								
16. DISTRIBUTION STATEMENT (of this Report) Approved for public release; distribution unlimited.										
17. DISTRIBUTION STATEMENT (of the abstract entered in Block 20, if different from Report)										
18. SUPPLEMENTARY NOTES										
19. KEY WORDS (Continue on reverse side if necessary and identify by block number) <table border="0" style="width: 100%;"> <tr> <td>Acoustic Plane Waves</td> <td>Inversion</td> </tr> <tr> <td>Forward Scattering Approximation</td> <td>Reflection Coefficient</td> </tr> <tr> <td>Grazing Angles</td> <td>Sound Speed Profiles</td> </tr> <tr> <td>Local Wave Decomposition</td> <td></td> </tr> </table>			Acoustic Plane Waves	Inversion	Forward Scattering Approximation	Reflection Coefficient	Grazing Angles	Sound Speed Profiles	Local Wave Decomposition	
Acoustic Plane Waves	Inversion									
Forward Scattering Approximation	Reflection Coefficient									
Grazing Angles	Sound Speed Profiles									
Local Wave Decomposition										
20. ABSTRACT (Continue on reverse side if necessary and identify by block number) <p>The implementation of a recently proposed inversion scheme for the scattering of acoustic plane waves by a layered ocean bottom is described. As a result of applying the forward scattering approximation to a local wave decomposition of the acoustic field, the reflection coefficient is obtained as a nonlinear Fourier transform of the logarithmic derivative of admittance. Inversion of the integral transform enables the recovery of admittance versus depth via numerical integration of the impulse</p>										

20. Cont'd.

response of the sea bottom. Separate recovery of both density and sound speed profiles requires two impulse responses corresponding to two distinct grazing angles. The capability of the inversion scheme is illustrated for three inhomogeneous models for which bandlimited impulse responses were generated synthetically.

TABLE OF CONTENTS

	Page
LIST OF ILLUSTRATIONS	iii
1. INTRODUCTION	1
2. THE FORWARD PROBLEM	3
2.1 The Mathematical Model	3
2.2 Global Field Equations	3
2.3 Local Field Equations	5
2.4 Integral Equation Representation	6
3. FORWARD SCATTERING APPROXIMATION	8
4. WKBJ APPROXIMATION	10
5. THE INVERSE SOLUTION	13
5.1 Physical Interpretation	13
5.2 The Inversion Formulas	13
5.3 Remarks	17
6. NUMERICAL RESULTS	19
6.1 Model 1	20
6.2 Model 2	26
6.3 Model 3	33
7. SUMMARY	41
8. REFERENCES	43
APPENDIX -- A RICATTI EQUATION FOR U/D	45

Accession For	
DTIC	1
COPY	1
INSPECTED	1



A

LIST OF ILLUSTRATIONS

Figure		Page
1	Mathematical Model	3
2	Density $\rho(\text{g/cm}^3)$ and Sound Speed $c(\text{m/s})$ Profiles as a Function of Depth $z(\text{m})$ for the Three Inhomogeneous Models Used in the Calculations	21
3	(a) Amplitude and (b) Phase of the Passband Frequency Response of the Reflection Coefficient for Model 1, Grazing Angle $\theta_0 = 60^\circ$..	22
4	(a) Amplitude and (b) Phase of the Passband Frequency Response of the Reflection Coefficient for Model 1, Grazing Angle $\theta_0 = 90^\circ$..	23
5	Bandlimited (0-64 Hz) Time Responses of the Reflection Coefficients for Model 1 at Grazing Angles (a) $\theta_0 = 60^\circ$ and (b) $\theta_0 = 90^\circ$, Rectangular Window Filter	24
6	Reconstructed Profiles for Model 1 Using the Time Responses in Figure 5 Showing (a) Normalized Density and (b) Refractive Index ...	25
7	(a) Amplitude and (b) Phase of the Passband Frequency Response of the Reflection Coefficient for Model 2, Grazing Angle $\theta_0 = 60^\circ$..	27
8	(a) Amplitude and (b) Phase of the Passband Frequency Response of the Reflection Coefficient for Model 2, Grazing Angle $\theta_0 = 90^\circ$..	28
9	Bandlimited (0-64 Hz) Time Responses of the Reflection Coefficients for Model 2 at Grazing Angles (a) $\theta_0 = 60^\circ$ and (b) $\theta_0 = 90^\circ$, Rectangular Window Filter	29
10	Reconstructed Profiles for Model 2 Using the Time Responses in Figure 9 Showing (a) Normalized Density and (b) Refractive Index ...	30
11	Bandlimited (0-64 Hz) Time Responses of the Reflection Coefficients for Model 2 at Grazing Angles (a) $\theta_0 = 60^\circ$ and (b) $\theta_0 = 90^\circ$, Kaiser Window Filter	31
12	Reconstructed Profiles for Model 2 Using the Time Responses in Figure 11 Showing (a) Normalized Density and (b) Refractive Index ..	32
13	(a) Amplitude and (b) Phase of the Passband Frequency Response of the Reflection Coefficient for Model 3, Grazing Angle $\theta_0 = 60^\circ$..	34
14	(a) Amplitude and (b) Phase of the Passband Frequency Response of the Reflection Coefficient for Model 3, Grazing Angle $\theta_0 = 90^\circ$..	35
15	Bandlimited (0-64 Hz) Time Responses of the Reflection Coefficients for Model 3 at Grazing Angles (a) $\theta_0 = 60^\circ$ and (b) $\theta_0 = 90^\circ$, Rectangular Window Filter	36

LIST OF ILLUSTRATIONS (Cont'd)

Figure	Page
16 Reconstructed Profiles for Model 3 Using the Time Responses in Figure 15 Showing (a) Normalized Density and (b) Refractive Index ..	37
17 Bandlimited (0-64 Hz) Time Responses of the Reflection Coefficients for Model 3 at Grazing Angles (a) $\theta_0 = 60^\circ$ and (b) $\theta_0 = 90^\circ$, Kaiser Window Filter	38
18 Reconstructed Profiles for Model 3 Using the Time Responses in Figure 17 Showing (a) Normalized Density and (b) Refractive Index ..	39

INVERSION OF THE ACOUSTIC PLANE WAVE
REFLECTION RESPONSE OF A LAYERED OCEAN BOTTOM

1. INTRODUCTION

Proper interpretation of acoustic signals measured at sea often requires that their interaction within the ocean bottom be considered. This is particularly true at the low frequencies used in passive sonar applications since long wavelength sound waves can penetrate the surficial sediments. The effect of a layered ocean bottom on acoustic propagation is usually treated in terms of bottom loss, defined as the ratio of reflected to incident plane wave intensities expressed in decibels, as a function of frequency and grazing angle.

Estimates of bottom structure (e.g., density and sound speed profiles) can be obtained by comparing the bottom loss inferred from experiments with that calculated for idealized geoacoustic models. Parameters of the geoacoustic models are adjusted until calculated values of bottom loss agree with measured values according to criteria specified for this curve-fitting approach. Experimental bottom loss is often inferred from propagation measurements in which small explosive charges are used as sound sources. Although explosives provide the required broadband frequency response, their point-source distribution can give rise to multipaths in the subbottom that complicate determination of the bottom loss. Difficulties in interpretation occur at those source/receiver offsets for which subbottom refracted arrivals become time-coincident with arrivals reflected from the water/sediment interface.¹

The mathematical formulation whereby bottom loss is determined from a specification of the layered bottom structure is a well-posed problem of the "forward" type. The aim of investigations of bottom loss is a solution of the "inverse" problem, whereby the structure of the ocean bottom is determined from a limited knowledge of the bottom loss. Much of the theoretical effort on the inverse problem has been confined to the model of plane waves scattered by a one-dimensional inhomogeneous medium.

Two comprehensive reviews of formal results on one-dimensional inverse theory are given by Burridge² and Newton.³ Most of the effort has concentrated on exact methods of inversion, and few numerical results on simulated or real data have appeared. An exception is found in the recent work of Candel et al.^{4,5} In their method, the acoustic field is first split into upgoing and downgoing waves.⁶ Application of the forward scattering approximation leads, in a straightforward way, to an analytical expression for the reflection coefficient in the form of a nonlinear Fourier transform of the logarithmic derivative of the admittance. Inversion of the integral transform leads to a direct (noniterative) numerical algorithm for determining admittance as a function of depth from the impulse response of the medium.

In this report, we present the results to date on our implementation of the inversion technique proposed by Candel et al.^{4,5} for simulated data.

Other promising numerical inversion schemes that have appeared in the recent literature⁷⁻¹² are not discussed. In section 2 we review Candell et al.'s treatment of the forward problem for global and local wave representations and develop an equivalent integral equation form. In section 3 we develop an analytic expression for the reflection coefficient based on the forward scattering approximation. The same result is obtained in section 4 from WKBJ theory. A brief development of the Ricatti equation satisfied by the reflection coefficient is presented in the appendix. In section 5 we indicate how the approximate expression for the reflection coefficient leads to an efficient inversion method. After some discussion on implementation of the inversion algorithm, we present several numerical examples on simulated data to illustrate the method in section 6.

2. THE FORWARD PROBLEM

2.1 THE MATHEMATICAL MODEL

The mathematical model to be considered is shown in figure 1. An inhomogeneous liquid with density, $\rho(z)$, and sound speed, $c(z)$, which are arbitrary functions of depth, occupies the region $0 < z < H$ between two homogeneous liquids. It is convenient to regard the region $0 < z < H$ as divided into M layers of thickness, h_m , $m = 1, 2, \dots, M$. The density and sound speed within each layer are taken to vary continuously with discontinuities in $\rho(z)$ and $c(z)$ introduced at layer boundaries. The homogeneous regions are characterized by constant density and sound speed pairs ρ_0, c_0 for $z < 0$ and ρ_1, c_1 for $z > H$. All regions are assumed to be nonabsorbing.

An acoustic plane wave, p_i , initially propagating downward at a grazing angle θ_0 to the $z = 0$ plane, encounters the inhomogeneous medium at $z = 0$. Within $0 < z < H$, the incident wave is partially reflected and a reflected wave $R p_r$ is returned to $z < 0$. For $z > H$, where no further reflections occur, only a transmitted wave $T p_t$ continues to propagate.

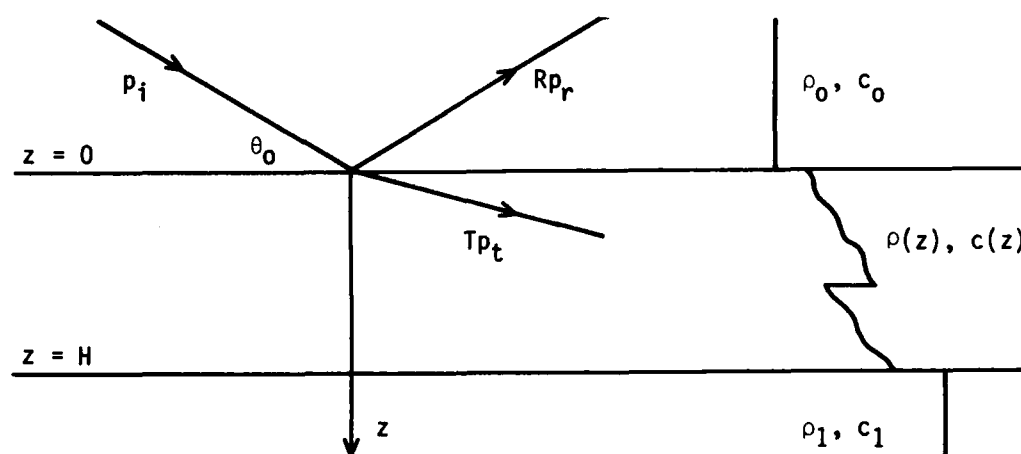


Figure 1. Mathematical Model

2.2 GLOBAL FIELD EQUATIONS

For stratified media, the wave vectors are confined to, say, the xz -plane, so that all field quantities are independent of y . Moreover, all waves exhibit a common wavenumber in the x -direction, i.e., $k_x = k_0 \cos \theta_0$, fixed by the angle of the incident wave. Assuming time-harmonic waves with angular frequency $\omega = 2\pi f$, the pressure and particle velocity can be represented by $p(z)\exp(ik_x x - i\omega t)$ and $[u(z), 0, w(z)]\exp(ik_x x - i\omega t)$, respectively. It follows that the basic equations describing the acoustic field in an inhomogeneous medium¹³ reduce to the form,

$$p' = i\omega\rho w, \quad (1)$$

$$w' = ik_z Y_z p, \quad (2)$$

$$u = k_x p / (\omega\rho), \quad (3)$$

where the prime denotes d/dz and $k_z = (k^2 - k_x^2)^{1/2}$ is the longitudinal component of the total wavenumber $k = \omega/c$ at a given depth z . Y_z defines a "longitudinal admittance,"

$$Y_z = (k_z/k) / (\rho c) = k_z / (\omega\rho). \quad (4)$$

For a plane wave propagating in a uniform medium with (real) wavenumbers k_x and k_z , Y_z is the ratio w/p for a downgoing wave and $-w/p$ for an upgoing wave. At normal incidence ($\theta_0 = 90^\circ$), $k_z = k$ and Y_z reduces to $Y = 1/(\rho c)$. Equations (1) and (2) can be cast into the compact matrix form,

$$\begin{pmatrix} p' \\ w' \end{pmatrix} = \begin{pmatrix} 0 & i\omega\rho \\ ik_z Y_z & 0 \end{pmatrix} \begin{pmatrix} p \\ w \end{pmatrix}. \quad (5)$$

We consider only the case for which k_z remains real everywhere, i.e., no total reflection occurs within the inhomogeneous region. Then the only wave propagating in $z > H$ can be represented by

$$p(z) = P \exp[ik_z(z - H)], \quad (6)$$

$$w(z) = W \exp[ik_z(z - H)]. \quad (7)$$

From equation (2) it follows that $ik_z W = ik_z Y_z P$, whence $W = Y_z P$. If we normalize P to unity, then appropriate initial conditions for the system in equation (5) are

$$p(H) = 1, \quad (8)$$

$$w(H) = Y_z(H). \quad (9)$$

With the above initial conditions, $p(z)$ and $w(z)$ can be calculated everywhere within $0 < z < H$ by numerically integrating the system in equation (5). The reflection and transmission coefficients may be obtained by letting A and B designate the incident and reflected amplitudes in $z < 0$. Then the field in this homogeneous region is represented by

$$p(z) = A \exp(ik_z z) + B \exp(-ik_z z), \quad (10)$$

where $k_z = (k_0^2 - k_x^2)^{1/2}$. According to equation (2),

$$w(z) = Y_z [A \exp(ik_z z) - B \exp(-ik_z z)]. \quad (11)$$

Solving equations (10) and (11) for A and B and evaluating at $z = 0$ gives

$$A = [p(0) + w(0)/Y_z(0)]/2, \quad (12)$$

$$B = [p(0) - w(0)/Y_z(0)]/2. \quad (13)$$

The reflection and transmission coefficients are then determined by

$$R = B/A = [p(0) - w(0)/Y_Z(0)]/[p(0) + w(0)/Y_Z(0)], \quad (14)$$

$$T = 1/A = 2/[p(0) + w(0)/Y_Z(0)]. \quad (15)$$

2.3 LOCAL FIELD EQUATIONS

The system in equation (5) together with initial conditions (8) and (9) provides a formal solution to the global evolution of the field. It is useful to obtain an alternate representation in terms of local waves, i.e., at each depth z to decompose the total field into upgoing and downgoing components. Although such a decomposition is not unique for inhomogeneous media,^{14,15} conditions for which reflected wave amplitudes are small relative to the incident wave amplitude suggest splitting the field into local waves as if the medium were locally homogeneous.

At each depth, we introduce a local upgoing wave, U , and a local downgoing wave, D , defined by

$$D = (p + w/Y_Z)/2, \quad (16)$$

$$U = (p - w/Y_Z)/2. \quad (17)$$

While the above decomposition is somewhat arbitrary for inhomogeneous media, it is a classical one.^{6,13,16,17} For homogeneous media, the splitting defined by equations (16) and (17) provides the desired identification of two elementary waves, as indicated by substitution into equations (10) and (11).

Equations (16) and (17) are readily inverted to give

$$p = D + U, \quad (18)$$

$$w = Y_Z(D - U). \quad (19)$$

Substitution of equations (18) and (19) into the coupled system (5) determines a new coupled system for the local fields U and D in the form

$$\begin{pmatrix} D' \\ U' \end{pmatrix} = \begin{pmatrix} ik_Z & 0 \\ 0 & -ik_Z \end{pmatrix} \begin{pmatrix} D \\ U \end{pmatrix} - g \begin{pmatrix} 1 & -1 \\ -1 & 1 \end{pmatrix} \begin{pmatrix} D \\ U \end{pmatrix}, \quad (20)$$

where we have set

$$g = Y_Z'/(2Y_Z) = (\ln Y_Z)'/2. \quad (21)$$

When the medium is homogeneous, the system in equation (20) decouples and U and D take the usual form of upgoing and downgoing waves. When the medium is inhomogeneous, coupling between U and D arises via g , the relative variation of the longitudinal admittance.

Integration of the system in equation (20) can be started at $z = H$. Below that depth, the only wave is downgoing. Choosing the downgoing amplitude as unity determines the initial conditions,

$$D(H) = 1, \quad (22)$$

$$U(H) = 0, \quad (23)$$

for the system in equation (20), which accord with conditions (8) and (9) for the system in equation (5) obtained earlier. Since $U(z)$ and $D(z)$ are determined at every depth z by numerical integration, it is reasonable to define local reflection and transmission coefficients as

$$R(z) = U(z)/D(z), \quad (24)$$

$$T(z) = 1/D(z). \quad (25)$$

The global field quantities p and w are continuous across discontinuities in the properties of the medium. The local waves U and D , however, are discontinuous there. Accordingly, some care is required when discontinuities in density and/or sound speed are encountered during the integration of the system in equation (20). Suppose an admittance jump of magnitude $Y_+ - Y_-$ occurs at depth z_0 , where $Y_{\pm} = Y_z(z_0 \pm 0)$. Then the continuity of p and w together with equations (18) and (19) determines the local wave U_- and D_- at $z_0 - 0$ in terms of the local waves U_+ and D_+ at $z_0 + 0$ according to

$$p_- = D_- + U_- = D_+ + U_+ = p_+, \quad (26)$$

$$w_- = Y_-(D_- - U_-) = Y_+(D_+ - U_+) = w_+, \quad (27)$$

from which the required jump conditions on the local waves are found to be

$$D_- = D_+(1 + Y_+/Y_-)/2 + U_+(1 - Y_+/Y_-)/2, \quad (28)$$

$$U_- = D_+(1 - Y_+/Y_-)/2 + U_+(1 + Y_+/Y_-)/2. \quad (29)$$

2.4 INTEGRAL EQUATION REPRESENTATION

The system in equation (20) can be rearranged into the alternate form,

$$\begin{pmatrix} D' \\ U' \end{pmatrix} = \begin{pmatrix} g_+ & g \\ g & g_- \end{pmatrix} \begin{pmatrix} D \\ U \end{pmatrix}, \quad (30)$$

where

$$g_{\pm} = -g \pm ik_z. \quad (31)$$

The differential system in equation (30) together with initial conditions in equations (22) and (23) can be converted into an equivalent integral form, e.g., by the variation of parameters method, to obtain

$$D(z) = \exp[f_+(z)] \left(1 + \int_H^z g(s) U(s) \exp[-f_+(s)] ds, \right) \quad (32)$$

$$U(z) = \exp[f_-(z)] \int_H^z g(s) D(s) \exp[-f_-(s)] ds, \quad (33)$$

where

$$f_{\pm}(z) = \int_H^z g_{\pm}(s) ds. \quad (34)$$

To this point the theory is exact. Approximations to U and D are now developed, leading to a useful analytic result for R , which forms the basis of a noniterative method of profile inversion. It is worthwhile noting that, whereas the local waves U and D satisfy the differential system in equation (20), the reflection coefficient $R = U/D$ satisfies a nonlinear equation of the Ricatti type. This point is developed briefly in the appendix.

3. FORWARD SCATTERING APPROXIMATION

While the differential system in equation (20) is readily solved numerically, an interesting approximation method may be developed that leads, in a straightforward way, to an analytic representation for the reflection coefficient. It is convenient to derive this result by solving equations (32) and (33) by successive approximations. In this scheme, higher order iterates $U(i+1)$ and $D(i+1)$ are obtained from previous ones, $U(i)$ and $D(i)$, by substituting the latter values into the right-hand side of equations (32) and (33). Candell et al.⁴ initiate the procedure by using a forward scattering approximation. This consists of, first, neglecting the upgoing wave U from equation (32), solving for D , and then using the D obtained in this step in equation (33) and solving for U . Although it is clearly possible to continue iterating in this fashion, for $|U| \ll |D|$ it is useful to examine the approximate solution obtained at this stage. In the approach just described, the differential system in equation (20) is replaced with a system for which the upper off-diagonal element -1 on the right-hand side is replaced by zero.

From equation (32) with $U(0) = 0$, the solution for $D(0)$ is found to be

$$D^{(0)}(z) = \exp[f_+(z)] = [Y_z(H)/Y_z]^{1/2} \exp[i \int_H^z k_z(s) ds]. \quad (35)$$

Substitution of equation (35) into the right-hand side of equation (33) leads to the solution for $U(1)$ in the form

$$U^{(1)}(z) = \exp[f_-(z)] \int_H^z g(s) \exp[2i \int_H^s k_z(t) dt] ds. \quad (36)$$

A useful approximation for the local reflection coefficient can now be obtained from equations (35) and (36) by forming the ratio $U^{(1)}(z)/D^{(0)}(z)$. The result evaluated at $z = 0$ is

$$R^{(1)}(0) = - \int_0^H g(s) \exp[2i \int_0^s k_z(t) dt] ds, \quad (37)$$

where the limits of integration have been altered according to

$$\int_H^S = \int_H^z + \int_z^S.$$

Although equation (37) is an approximation, it has been shown numerically⁴ to provide accurate results in many situations of practical interest. Moreover, this simple result obtained from the forward scattering approximation forms the basis of a method to recover the admittance versus depth of an inhomogeneous medium from the impulse response. We will develop the formalism of this method in a subsequent section.

It is shown in the appendix that equation (37) follows from the Ricatti equation formulation for $R = U/D$. Before proceeding to the development of the inversion approach from equation (37), it is worthwhile to examine this result within the context of the WKBJ approximation.

4. WKBJ APPROXIMATION

The approximation given by equation (37) has been derived elsewhere.^{8,13,14} It can be developed from a WKBJ representation for the solution in the region $0 < z < H$. The appropriate WKBJ form for the acoustic problem is

$$p(z) = A(z)W_+(z) + B(z)W_-(z), \quad (38)$$

where $A(z)$ and $B(z)$ are functions to be determined and

$$W_{\pm}(z) = \exp[\pm i \int_H^z k_z(s) ds] / [Y_z(z)]^{1/2}. \quad (39)$$

(W_{\pm} is not to be confused with the amplitude of the particle velocity used in section 2.2.) We recall that since we are only considering real propagating waves, the denominator of equation (39) is well defined throughout $0 < z < H$.

A coupled system of differential equations for A and B is readily obtained by direct manipulation.¹⁶ With the identification $D = AW_+$ and $U = BW_-$, there follows from equations (30), (31), (38), and (39) the sequence

$$\begin{aligned} D' &= (-g + ik_z)D + gU \\ &= (W'_+/W_+)D + gU \\ &= AW'_+ + gBW_- = A'W_+ + AW'_+, \end{aligned}$$

which determines the result

$$A' = gBY_z W_-^2. \quad (40)$$

The result for B' is obtained in a similar way. The final coupled system for A and B can be expressed in the compact matrix form,

$$\begin{pmatrix} A' \\ B' \end{pmatrix} = \begin{pmatrix} 0 & gY_z W_-^2 \\ gY_z W_+^2 & 0 \end{pmatrix} \begin{pmatrix} A \\ B \end{pmatrix}. \quad (41)$$

From the initial conditions for U and D , it follows that appropriate initial conditions for the system in equation (41) are given by

$$A(H) = [Y_z(H)]^{1/2}, \quad (42)$$

$$B(H) = 0. \quad (43)$$

The above initial conditions are readily incorporated into the integral equation form equivalent to the differential system in equation (41), i.e.,

$$A(z) = [Y_z(H)]^{1/2} + \int_H^z g(s) B(s) \exp[-2i \int_H^s k_z(t) dt] ds, \quad (44)$$

$$B(z) = \int_H^z g(s) A(s) \exp[+2i \int_H^s k_z(t) dt] ds, \quad (45)$$

The usual assumption invoked in attempting a solution of the WKBJ form given by equations (38) and (39) is that variations in the medium are slow compared with the wavelength of the waves. Under these conditions, the relative variation of longitudinal admittance $|g| \ll 1$ and the system in equations (44) and (45) can be solved by successive approximation. Setting $g = 0$ initially leads to zeroth order estimates $A(0) = [Y_z(H)]^{1/2}$ and $B(0) = 0$. Substituting these results into the right-hand sides of equations (44) and (45), we find $A(1) = A(0)$ and

$$B^{(1)}(z) = [Y_z(H)]^{1/2} \int_H^z g(s) \exp[2i \int_H^s k_z(t) dt] ds. \quad (46)$$

The approximate first order reflection coefficient given by $R^{(1)} = (B^{(1)} W_-) / (A^{(1)} W_+)$ when evaluated at the surface $z = 0$ takes the form

$$R^{(1)}(0) = - \int_0^H g(s) \exp[2i \int_0^s k_z(t) dt] ds, \quad (47)$$

which agrees with the result obtained previously via the forward scattering approximation.

It is worthwhile remarking that the system in equation (41) can be solved numerically. McKisic and Hamm¹⁸ suggest one method. For the problems to be considered in the present work, with k_z everywhere real, a simple formulation is obtained by setting $C = Y_z^{1/2} W_+$, from which we obtain the system

$$\begin{pmatrix} A' \\ B' \\ C' \end{pmatrix} = \begin{pmatrix} 0 & g/C^2 & 0 \\ gC^2 & 0 & 0 \\ 0 & 0 & ik_z \end{pmatrix} \begin{pmatrix} A \\ B \\ C \end{pmatrix}, \quad (48)$$

subject to initial conditions

$$A(H) = [Y_z(H)]^{1/2}, \quad (49)$$

$$B(H) = 0, \quad (50)$$

$$C(H) = 1. \quad (51)$$

Jump conditions on A and B must be applied whenever discontinuities in Y_z are encountered. From equations (26) and (27) and the relationships $D = AC/Y_z^{1/2}$ and $U = B/(CY_z^{1/2})$, the required connections are readily deduced to be

$$A_- = [Y_-/Y_+]^{1/2} [A_+(1 + Y_+/Y_-)/2 + C^{-2} B_+(1 - Y_+/Y_-)/2], \quad (52)$$

$$B_- = [Y_-/Y_+]^{1/2} [C^2 A_+(1 - Y_+/Y_-)/2 + B_+(1 + Y_+/Y_-)/2], \quad (53)$$

where $C = C_- = C_+$.

5. THE INVERSE SOLUTION

5.1 PHYSICAL INTERPRETATION

Before proceeding with the development of the inversion scheme based on equation (37), it is worthwhile commenting on the physical interpretation of this approximate result. Since all subsequent work will focus on the reflection coefficient at $z = 0$, we drop the depth dependence from the argument of R and replace it with the frequency dependence since it is apparent that R depends on f via the parameter k_z .

The reflection coefficient in equation (37) appears as a sum of contributions from successive elementary layers. About the layer at depth $z = z_0$, we obtain a partial reflection coefficient,

$$dR(f) = -g(z_0) \exp\left[2i \int_0^{z_0} k_z(s) ds\right] dz_0,$$

with an amplitude determined by the relative variation of longitudinal admittance at that depth and a phase,

$$\phi(f) = 2 \int_0^{z_0} k_z(s) ds,$$

associated with the time taken for the incident wave to travel to depth $z = z_0$ and to return to depth $z = 0$ as a partially reflected wave. This is seen more clearly by writing $\phi(f) = 2\pi f\tau$, where

$$\tau = 2 \int_0^{z_0} ds/c_z(s) \quad (54)$$

is the total propagation time from $z = 0$ to $z = z_0$ and back for a wave having longitudinal phase speed $c_z = \omega/k_z$.

5.2 THE INVERSION FORMULAS

We observe that equation (37) determines the reflection coefficient as a nonlinear Fourier transform. Inverting this Fourier transform recovers the relative variation of the longitudinal admittance and integration determines the admittance itself. We remark here that only Y_z can be recovered from a knowledge of $R(f)$ for a given angle of incidence. Independent determination of both the density, ρ , and the sound speed, c , requires more information. We will return to this point later.

To cast equation (37) in the form of a standard Fourier transform, we introduce a new coordinate ζ defined by

$$\zeta = (2/k_0) \int_0^z k_z(s) ds, \quad (55)$$

where k_0 designates the wavenumber in region $z < 0$. With the above change of variable, we obtain the result

$$R(f) = - \int_0^{\zeta(H)} g(\zeta) \exp(2\pi i f \zeta / c_0) d\zeta, \quad (56)$$

where $g(\zeta) = Y'_z(\zeta) / [2Y_z(\zeta)]$ and the prime is now used to denote $d/d\zeta$. The reflection coefficient now appears as a standard Fourier transform of the relative variation of longitudinal admittance with respect to the new variable ζ .

To invert equation (56) we first compute the time response of the medium, i.e., the reflection coefficient as a function of time given by

$$r(t) = \int_{-\infty}^{\infty} R(f) \exp(-2\pi i f t) df. \quad (57)$$

Transforming both sides of equation (56) leads to the result

$$r(t) = - \int_0^{\zeta(H)} \int_{-\infty}^{\infty} g(\zeta) \exp[2\pi i f (\zeta / c_0 - t)] df d\zeta. \quad (58)$$

The integration with respect to f may be performed at once giving

$$\int_{-\infty}^{\infty} \exp[2\pi i f (\zeta / c_0 - t)] df = c_0 \delta(\zeta - c_0 t), \quad (59)$$

whence the sifting property of the delta function determines the time response in the form

$$r(t) = - c_0 g(c_0 t) = - c_0 [(dY_z/d\zeta) / (2Y_z)] \Big|_{\zeta = c_0 t}. \quad (60)$$

The physical interpretation of equation (60) indicates that the time response at instant t is proportional to the relative variation of admittance at the layer of coordinate $\zeta = c_0 t$ corresponding to an actual location given by

$$c_0 t = (2/k_0) \int_0^z k_z(s) ds \quad (61)$$

or

$$t = 2 \int_0^z ds / c_z(s). \quad (62)$$

The "active" layer at instant t is located at a distance z corresponding to the travel time from $z = 0$ to this layer and back.

Equation (60) may be rearranged in the form

$$\left. \frac{Y'_z}{Y_z} \right|_{z=c_0 t} = -2r(t)/c_0, \quad (63)$$

and equation (55) may be replaced by

$$z' = k_0/(2k_z) = 1/(2\rho c_0 Y_z), \quad (64)$$

where use was made of equation (4). Since these two relations (with appropriate initial conditions) allow the determination of Y_z versus z , the direct inversion scheme is formally complete.

The inversion algorithm of Candel et al.⁵ is formed from equations (4), (63), and (64). Three cases have to be considered separately.

5.2.1 Case A: $\rho(z)$ Known, $c(z)$ Unknown

When density $\rho(z)$ is known, the sound speed $c(z)$ can be determined by integrating equations (63) and (64) directly, i.e.,

$$Y'_z = -(2/c_0)rY_z, \quad (65)$$

$$z' = 1/(2\rho c_0 Y_z). \quad (66)$$

At each step of the numerical integration, the sound speed can be recovered from equation (4), which can be written in the convenient form

$$n = [\rho^2 c_0^2 Y_z^2 + \cos^2 \theta_0]^{1/2}, \quad (67)$$

where $n(z) = c_0/c(z) = k(z)/k_0$ is the local index of refraction and $\cos \theta_0 = k_x/k_0$ determines the grazing angle at $z = 0$. For a receiver located at $z = z_0$, corresponding to a point at $z = z_0$ in $z < 0$, the integration of equations (65) and (66) may be started with the initial conditions

$$Y_z(z_0) = \sin \theta_0/(\rho_0 c_0), \quad (68)$$

$$z_0 = \zeta_0/(2 \sin \theta_0). \quad (69)$$

5.2.2 Case B: $c(z)$ Known, $\rho(z)$ Unknown

For the case when the sound speed, $c(z)$, is known and the density, $\rho(z)$,

is to be determined, equations (4) and (64) have to be modified slightly, but equation (63) remains unchanged. We find

$$Y'_z = -(2/c_0)rY_z, \quad (70)$$

$$z' = [n^2 - \cos^2 \theta_0]^{-1/2}/2, \quad (71)$$

$$\rho = [n^2 - \cos^2 \theta_0]^{1/2}/(c_0 Y_z). \quad (72)$$

The system in equations (70) and (71) is directly integrable since $n(z)$ is known everywhere. At each step in the integration, the density is obtained simply from equation (72). The initial conditions for equations (70) and (71) are the same as in case A, subsection 5.2.1.

5.2.3 Case C: $\rho(z)$ and $c(z)$ Unknown

As indicated previously, unique determination of both density, $\rho(z)$, and sound speed, $c(z)$, requires additional information. For the application of Candel et al.'s⁵ inversion method, reflection responses for at least two distinct grazing angles must be provided.

Let the subscripts 1 and 2 denote the quantities that correspond to the two distinct grazing angles θ_1 and θ_2 , with $\theta_2 > \theta_1$. The relevant differential equation system for grazing angle θ_1 is given by

$$(Y_z)_1' = -(2/c_0)r_1(Y_z)_1, \quad (73)$$

$$z' = 1/[2\rho c_0(Y_z)_1], \quad (74)$$

$$(Y_z)_1 = [n^2 - \cos^2 \theta_1]^{1/2}/(\rho c_0), \quad (75)$$

where the prime now denotes $d/d\zeta_1$. A similar set of equations corresponds to the other grazing angle θ_2 , but it is apparent that the integration variables ζ_1 and ζ_2 are not identical. Use of the chain rule for differentiation, however, relates ζ_1 to ζ_2 so that the system for grazing angle θ_2 can be specified in terms of ζ_1 in the form

$$\zeta_2' = (Y_z)_2/(Y_z)_1, \quad (76)$$

$$(Y_z)_2' = -(2/c_0)r_2(Y_z)_2^2/(Y_z)_1, \quad (77)$$

$$(Y_z)_2 = [n^2 - \cos^2 \theta_2]^{1/2}/(\rho c_0). \quad (78)$$

Now ζ_2 is determined as a dependent variable that allows $(Y_z)_1$ and $(Y_z)_2$ to be determined at the same depth location z . The density and sound speed are then readily deduced by combining equations (75) and (78):

$$\rho^2 c_0^2 = [\cos^2 \theta_1 - \cos^2 \theta_2] / [(Y_z)_2^2 - (Y_z)_1^2], \quad (79)$$

$$n^2 = [(Y_z)_2^2 \cos^2 \theta_1 - (Y_z)_1^2 \cos^2 \theta_2] / [(Y_z)_2^2 - (Y_z)_1^2]. \quad (80)$$

It is evident that the integration of equation (74) can proceed only in conjunction with the determination of ρ via equation (79). Appropriate initial conditions for this case become

$$Y_z(\zeta_0)_1 = \sin \theta_1 / (\rho_0 c_0), \quad (81)$$

$$z_0 = \zeta_0 / (2 \sin \theta_1), \quad (82)$$

$$\zeta_2(\zeta_0) = \zeta_0 Y_z(\zeta_0)_2 / Y_z(\zeta_0)_1, \quad (83)$$

$$Y_z(\zeta_0)_2 = \sin \theta_2 / (\rho_0 c_0). \quad (84)$$

In principle, it is no more difficult to determine both the density, $\rho(z)$, and the sound speed, $c(z)$, profiles than one of them. However, reflection responses for at least two probing directions are required, and four instead of two differential equations must be integrated.

5.3 REMARKS

Before proceeding with numerical aspects of both the forward and inverse problems, some comments on the analysis so far are in order.

The steps leading to equation (6) required the relative variation of admittance to be independent of frequency. While this is most certainly a valid assumption for the density and sound speed, usual treatments regarding absorption presume at least a linear dependence on f . Therefore, absorption was taken to be zero in the above analysis. It may be possible to incorporate some frequency dependence into Y_z and still manipulate the integrands in a straightforward way, but that task will not be undertaken in this report.* Another reason for neglecting the effects of absorption lies in numerical difficulties associated with integrating differential equations containing a damping term.

The restriction to real propagating waves everywhere within the inhomogeneous region $0 < z < H$ is partly due to numerical difficulties associated with turning points within the domain of integration. Ad hoc devices are sometimes introduced to avoid numerical underflow/overflow

* In fact, if absorption in the subbottom is proportional to frequency, then Y_z remains independent of f .

problems in these situations.¹⁹ On the other hand, waves are exponentially attenuated below a turning point and quickly lose any practical capability to return information from regions at greater depths.

In the WKBJ approach to the approximate analytical representation for the reflection coefficient, the criterion $|g| \ll 1$ was used. This condition seems to preclude regions containing discontinuities of the first kind from consideration. However, the forward scattering approach of Candel et al.⁴ only assumes $|U| \ll |D|$, which can hold even in the presence of discontinuous jumps in material properties. Clearly the latter condition encompasses the former one. It is interesting that both criteria lead to the same approximate formula for the reflection coefficient.

The inversion scheme suggested by equations (63) and (64), which only requires integration of a pair of first order differential equations, together with equation (4), is direct since its implementation does not involve an iteration procedure. On the other hand, it would appear that the scheme only accounts for first order reflections from the inhomogeneous medium. This is partly because the mapping between the depth coordinate, z , and the time, t , is monotonic; i.e., later times correspond to deeper depths. For conditions in the subbottom, which support multiple scattering, the correspondence is not monotonic. Because of this limitation, configurations of material properties giving rise to multiple scattering should be monitored during the inversion process and their effect taken into account in the interpretation of results.

6. NUMERICAL RESULTS

In this section, we present some numerical results based on a computer implementation of Candel et al.'s⁵ inversion procedure for simulated data. Their numerical examples were restricted to waves propagating at normal incidence ($\theta_0 = 90^\circ$) in regions of constant density ($\rho(z) = \rho_0$) only, and recovery of $n(z)$ required only a single impulse response, $r(t)$. Here we extend the numerical results to incorporate two impulse responses corresponding to both normal and oblique grazing angles so that simultaneous recovery of both $n(z)$ and $\rho(z)$ is possible. For most applications to acoustic probing of the ocean bottom, both $n(z)$ and $\rho(z)$ are usually unknown.

For each model to be considered, the computer simulation is carried out in the following way. At a given grazing angle, the bandlimited frequency response $R(f)$ is determined for a finite set of discrete frequencies $f_k = k\Delta f$, $k = 0, 1, \dots, K-1$. The reflected time series $r(t_n)$, $t_n = n\Delta t$, $n = 0, 1, \dots, N-1$ is determined via a discrete inverse Fourier transform. The discrete transform is effected using a fast Fourier transform (FFT) algorithm. $N-K$ zeros are appended to each $R(f_k)$ response to enhance the resolution of $r(t_n)$ due to the FFT constraint, $\Delta t\Delta f = 1/N$. With r_1 and r_2 computed for distinct grazing angles θ_1 and θ_2 , with $\theta_2 > \theta_1$, recovery of $n(z)$ and $\rho(z)$ proceeds according to case C, subsection 5.2.3. Reconstructed $n(z)$ and $\rho(z)$ are finally compared with the refractive index and density profiles initially used to generate the synthetic responses.

For the forward problem, any of the four representations of the acoustic field (system in equation (5) for p and w ; system in equation (20) for D and U ; system in equation (48) for A , B , and C ; and equation (A-1) for R) together with appropriate initial and jump conditions can be used to determine the reflection coefficient. Experience with each system indicates that the representation in terms of the local waves D and U requires the least computational effort. For both the forward problem and its inverse solution, numerical integration of the relevant system of first order differential equations was carried out using a computer code developed by Shampine and Gordon.²⁰ This code is well documented and features automatic local error control. Moreover, it has been used successfully in other studies of plane wave reflection coefficients for layered geoacoustic models.²¹ To accommodate complex functions such as D and U appearing in the system in equation (20), it is first necessary to separate the equations into real and imaginary parts. In addition, for numerical work, it is recommended that all equations be converted to a dimensionless form. This is easily accomplished by introducing the scaled quantities $z^* = z/H$, $f^* = fH/c_0$, and $Y_z^* = \rho_0 c_0 Y_z$, where the scaling factors are the thickness of the inhomogeneous region, H , and the density, ρ_0 , and sound speed, c_0 , of the region $z < 0$. For the inverse problem, we also have $\zeta^* = \zeta/H = c_0 t/H = t^*$. As a result of this scaling, it was possible to maintain numerical accuracy using single precision arithmetic.

For the results presented in this section, the sound speed and density profiles within the inhomogeneous region $0 < z < H$ are modeled in the following way. For each model, the region $0 < z < H$ is divided into M layers

of thickness, h_m , $m = 1, 2, \dots, M$. Within the m th layer, the density is assumed to be constant while the variation of $c(z)$ is modeled according to $1/c(z) = a_m z + b_m$. The layer coefficients a_m and b_m are determined from the respective sound speeds at the top and bottom of the m th layer. With this prescription, the admittance varies linearly within each layer. Discontinuities in $c(z)$ or $\rho(z)$ can be introduced at layer interfaces.

Three models are considered in the numerical examples. Model 1 comprises a linear refractive index and constant density layer. Model 2 provides an example of a sudden discontinuity in both refractive index and density. Both of these models were discussed by Candel et al.^{4,5} Model 3 represents a geoacoustic model of Hatteras Abyssal Plain based on traditional seismic interpretation of time waveforms.²² The sound speed and density profiles for the three models are summarized in figure 2.

For each model, the complex frequency response $R = \text{Re}[R] + i \text{Im}[R]$ was computed at 256 discrete frequencies $f_k = k\Delta f$, $k = 0, 1, \dots, 255$, and $\Delta f = 0.5$ Hz for grazing angles 60° and 90° . The complex sequence $R(f)$ was extended to $N = 1024$ points by appending 512 zero values. Since the time response $r(t)$ is a real sequence, $R(f)$ satisfies the symmetry conditions $\text{Re}[R(-f)] = \text{Re}[R(f)]$ and $\text{Im}[R(-f)] = -\text{Im}[R(f)]$.^{5,23} Complex arithmetic was avoided by using an FFT algorithm specially designed to treat discrete transforms of real sequences and their inverses.^{23,24} The inverse FFT produced 1024 estimates of the time response at $t_n = n\Delta t$, $n = 0, 1, \dots, 1023$, where $\Delta t = 1/(N\Delta f) = 1/512$ seconds. Each time response was then convolved with a low-pass digital filter designed using the window method.²⁵ Filters using both rectangular and Kaiser windows were employed with a cutoff frequency of 64 Hz. Finally, the filtered time responses were multiplied by Δf to approximate the analytical Fourier transform results.^{5,23}

6.1 MODEL 1

Figures 3 and 4 depict the frequency responses of the reflection coefficient for model 1. The amplitude and phase of $R(f)$ are shown for a grazing angle of 60° in figure 3 and 90° in figure 4. For both grazing angles $|R|$ decreases globally with increasing frequency and exhibits weak oscillations. The phase increases monotonically but it is nonlinear. It is easy to see that $|R|$ is greater for oblique than for normal incidence. At zero frequency, the values of $|R|$ correspond to the values obtained for a sudden discontinuity in the sound speed of magnitude c_0/c_1 . This example is discussed in greater detail by Candel et al.^{4,5} for the case of normal incidence.

The time responses for model 1 are shown in figure 5. The upper trace corresponds to $\theta_0 = 60^\circ$ and the lower to $\theta_0 = 90^\circ$. Each response has been normalized by its peak value of r . The initial time offset corresponds to the two-way travel time for a receiver located at $z = -100$ m. The time delay $\tau_0 = (2z/c_0) \sin \theta_0$ is implemented by applying the complex modulation $\exp(-2\pi i f \tau_0)$ to $R(f)$ before taking the inverse Fourier transform. The smaller time delay for oblique incidence follows from equation (54) since the wave propagates at the longitudinal phase speed c_z . The initial rise in each trace is due to the discontinuity in the sound speed gradient at $z = 0$.

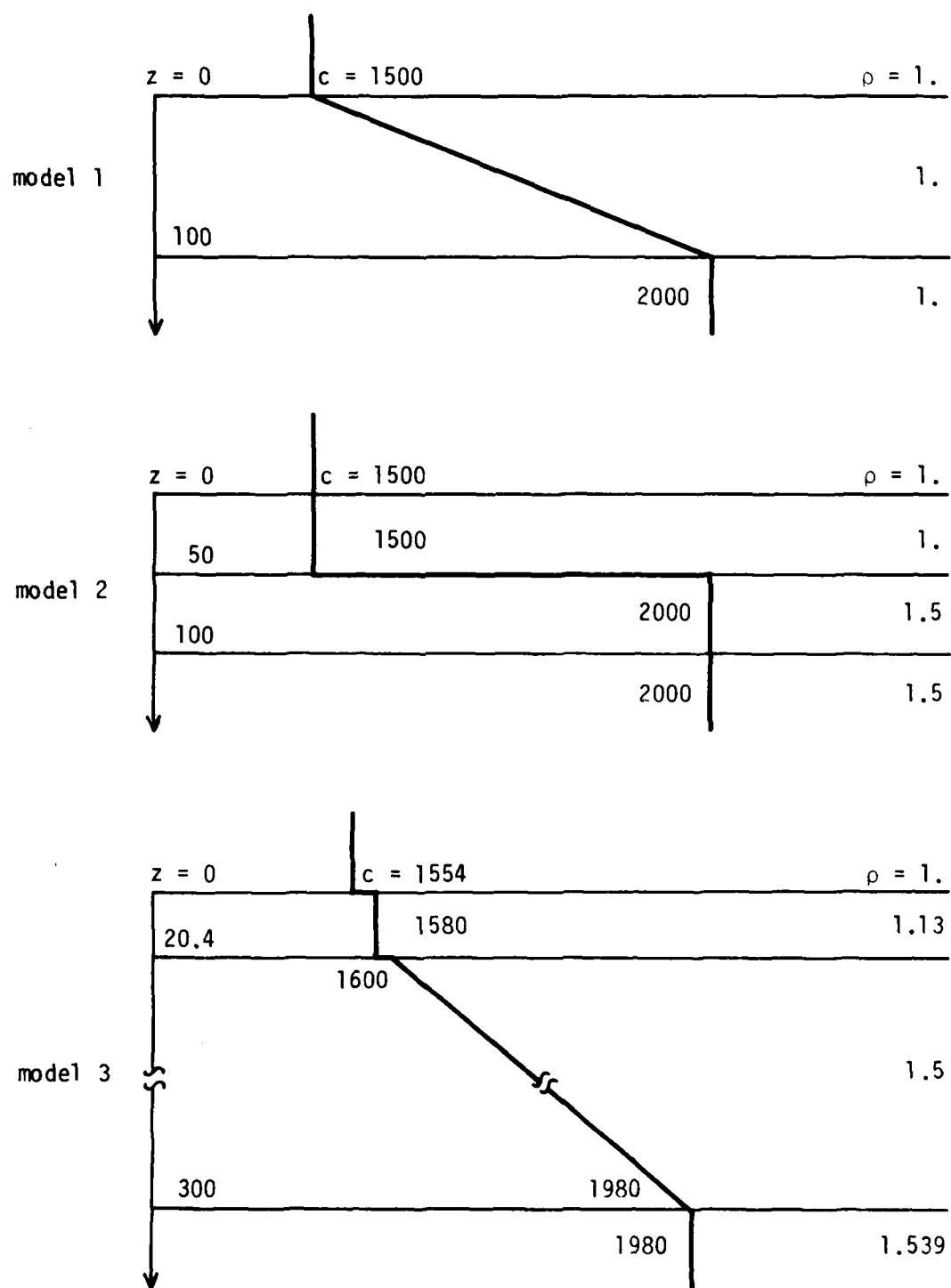


Figure 2. Density ρ (g/cm³) and Sound Speed c (m/s) Profiles as a Function of Depth z (m) for the Three Inhomogeneous Models Used in the Calculations

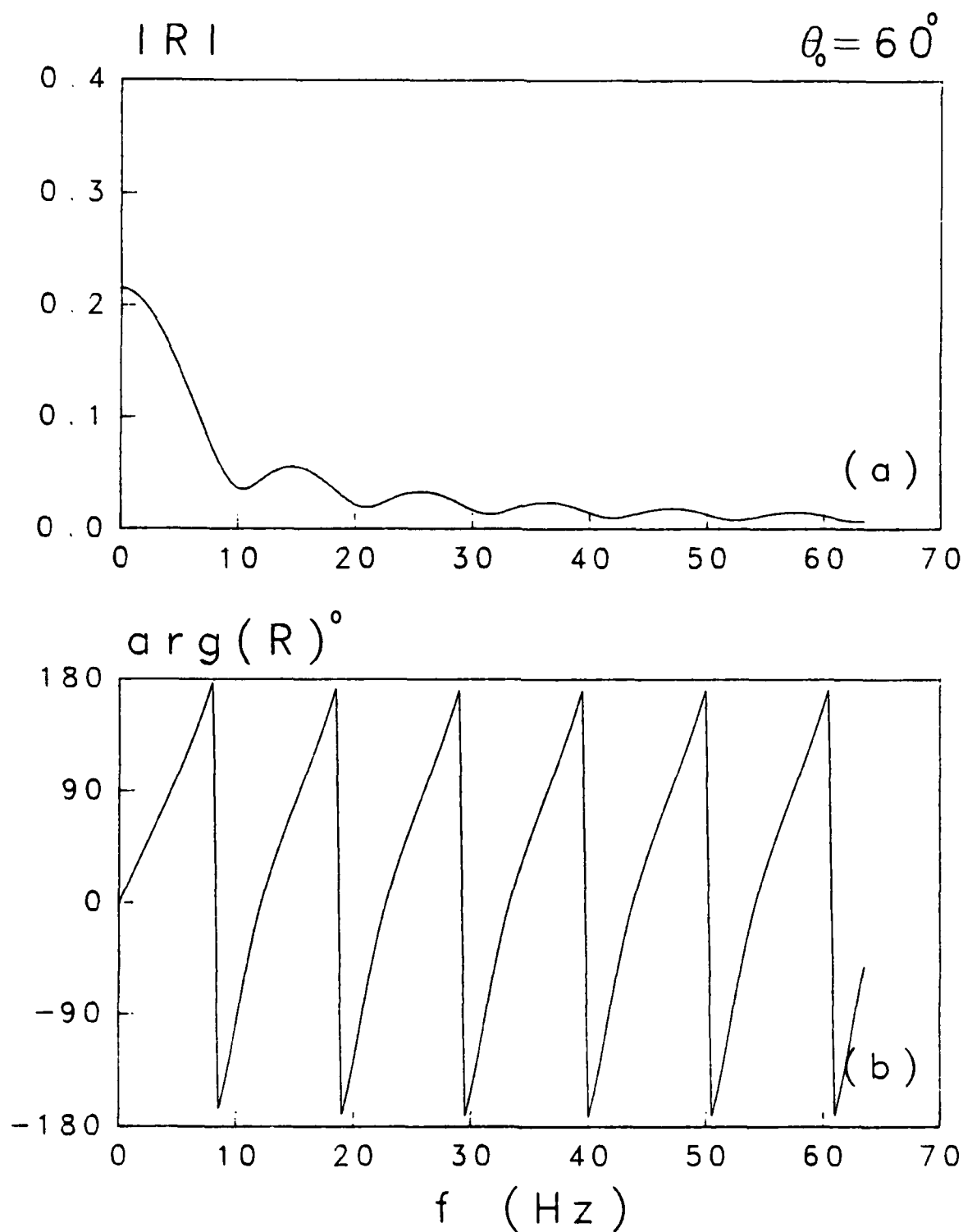


Figure 3. (a) Amplitude and (b) Phase of the Passband Frequency Response of the Reflection Coefficient for Model 1, Grazing Angle $\theta_0 = 60^\circ$

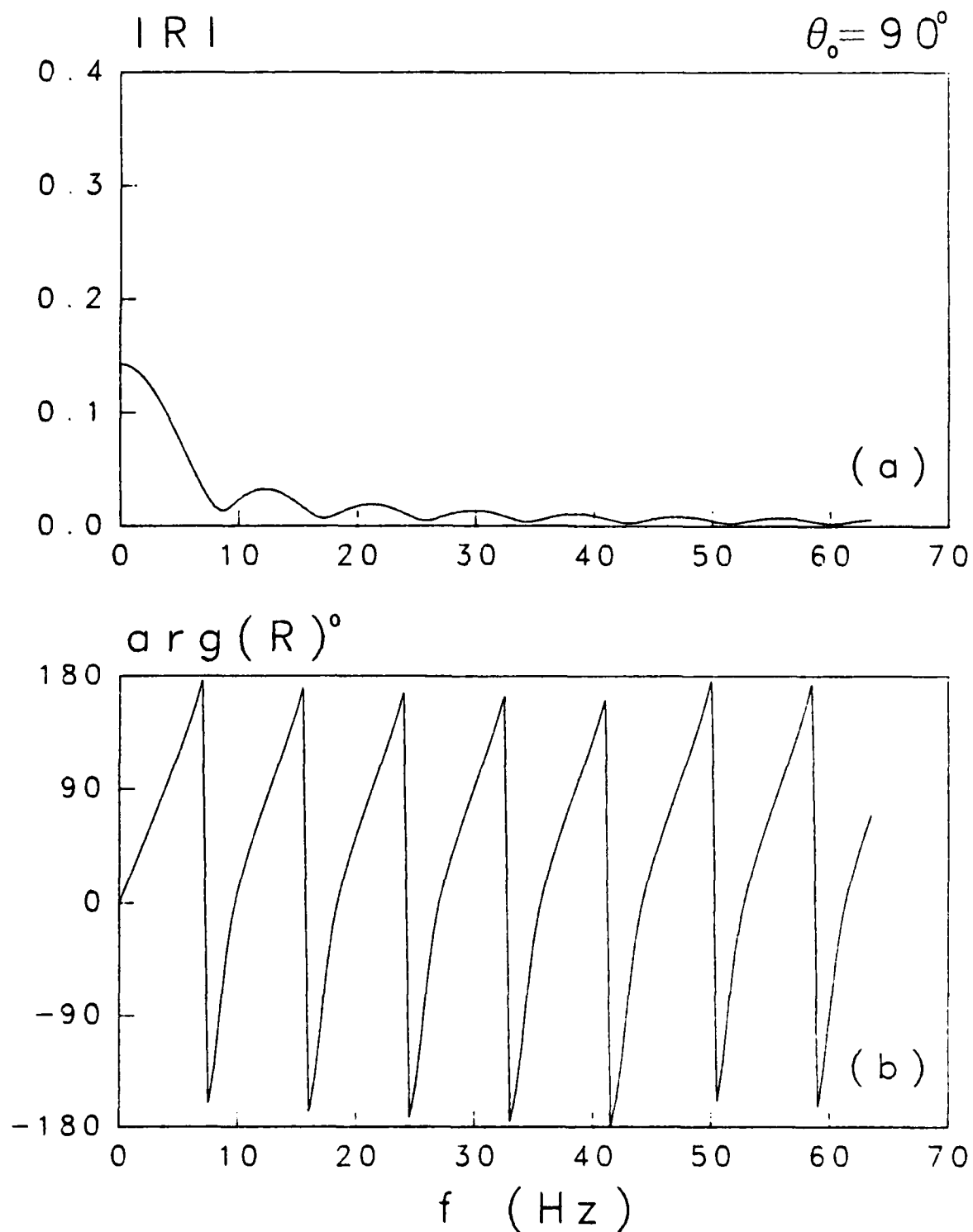


Figure 4. (a) Amplitude and (b) Phase of the Passband Frequency Response of the Reflection Coefficient for Model 1, Grazing Angle $\theta_0 = 90^\circ$

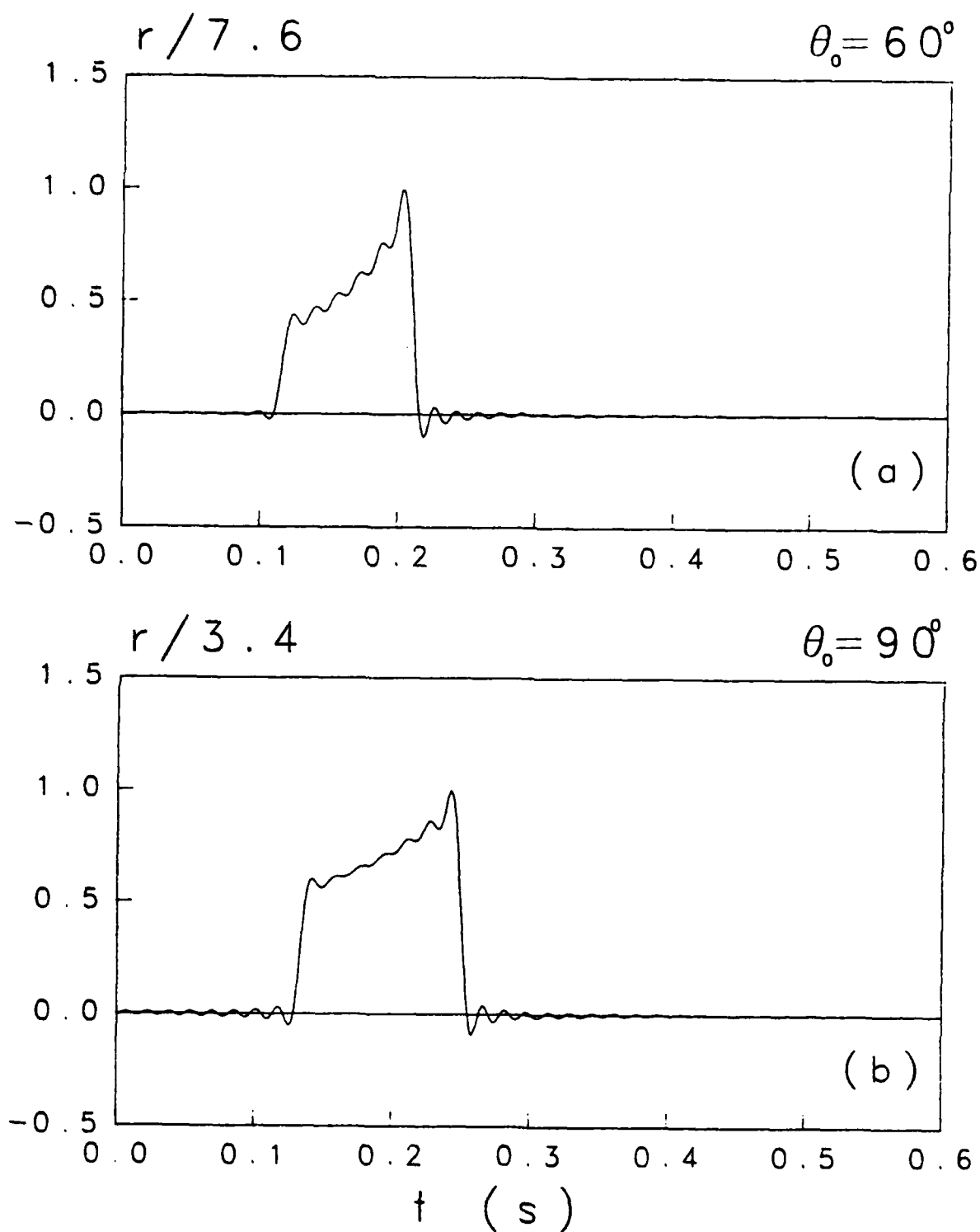


Figure 5. Bandlimited (0-64 Hz) Time Responses of the Reflection Coefficients for Model 1 at Grazing Angles (a) $\theta_0 = 60^\circ$ and (b) $\theta_0 = 90^\circ$, Rectangular Window Filter

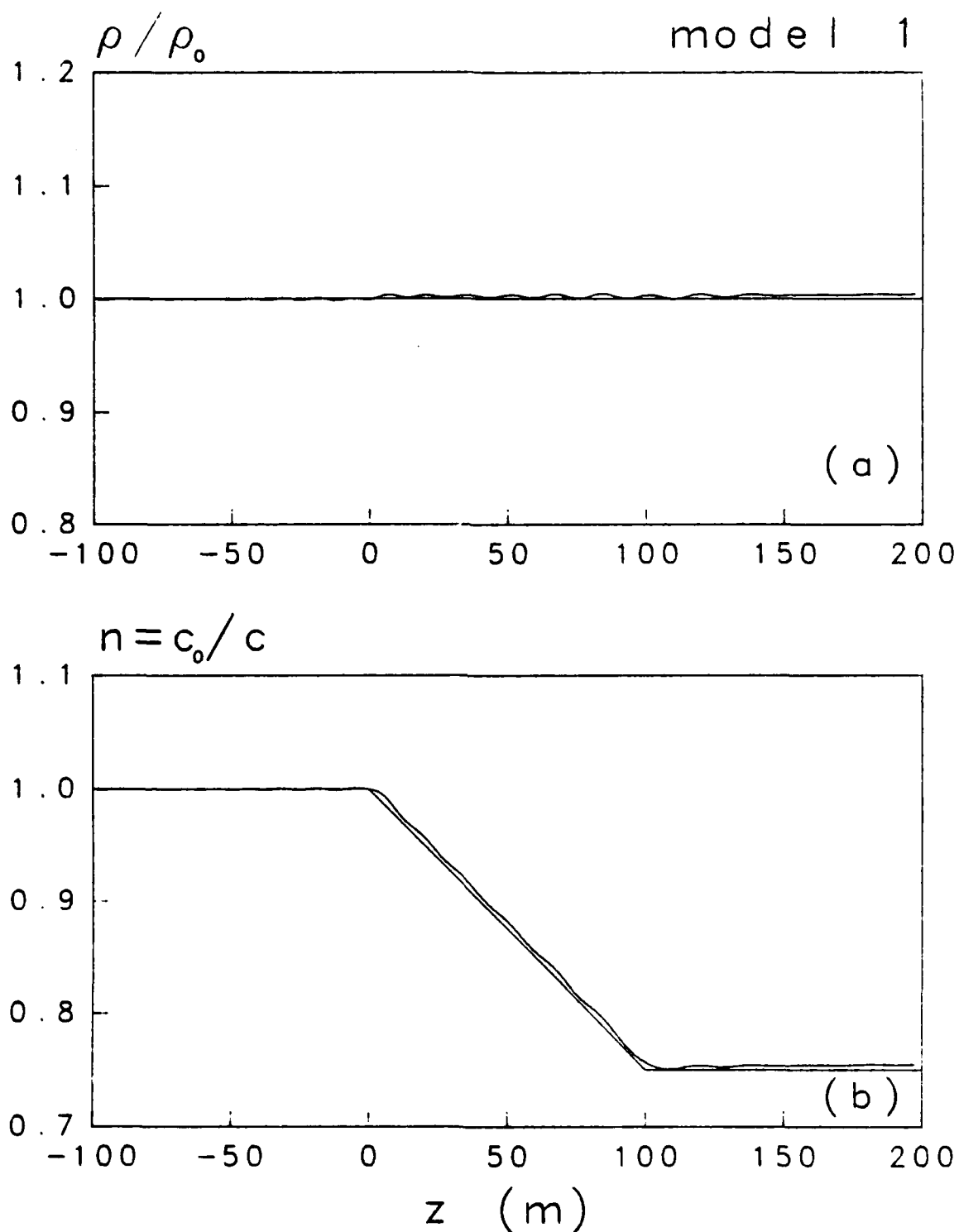


Figure 6. Reconstructed Profiles for Model 1 Using the Time Responses in Figure 5 Showing (a) Normalized Density and (b) Refractive Index

Continuous reflections are observed as the wave traverses the inhomogeneous layer. The duration of the time response is less for oblique incidence, but there is a greater peak response at the discontinuity in the sound speed gradient at $z = H$. The slight oscillations evident in both responses are a result of truncating the frequency responses with a rectangular window at the cutoff frequency of 64 Hz. The discontinuity in $R(f)$ generated by this filtering operation gives rise to the well-known Gibbs phenomenon.^{23,25} These oscillations are small for this example since $|R|$ is small at cutoff.

The inversion algorithm of Candel et al.⁵ was used to determine the reconstructed values of $\rho(z)$ and $n(z)$ in figure 6 from the time responses in figure 5. For comparison, the density and sound speed profiles of the model used to generate $R(f)$ are displayed on the same graphs. It is evident that the inversion scheme gives excellent results for this example.

6.2 MODEL 2

The frequency responses for the step-discontinuity profile of model 2 are shown in figures 7 and 8. In this example, both density and sound speed have a jump discontinuity at $z = 50$ m. The responses for $\theta_0 = 60^\circ$ and $\theta_0 = 90^\circ$ are given in figures 7 and 8, respectively. For this model, the analytical form of R is known,⁴ and the numerical results correctly reproduce the constant amplitude and linear phase behavior. The reflection amplitude is again greater for oblique incidence. The normalized time responses obtained using a rectangular window filter are shown in figure 9 for a receiver located at $z = -100$ m. As before, the peak response is larger and arrives earlier for oblique incidence. For this example, the discontinuity introduced by truncating R at 64 Hz produces significant Gibbs oscillations. Instead of a "pulse-like" arrival, a sinc-response⁵ is observed.

Figure 10 shows the reconstruction of $\rho(z)$ and $n(z)$ based on the time responses in figure 9. Although the reconstructed values reproduce the global behavior of the model values, the effect of the large Gibbs oscillations is apparent. Since these oscillations result from the discontinuity introduced by the rectangular filter, it is reasonable to design a filter to reduce this effect. Figure 11 shows time responses for model 2 after filtering with a Kaiser window filter. For these results, a 31-point filter with 60-dB sidelobe suppression was used.²⁵ It is evident that most of the effects of the truncation have been removed. The reconstruction based on the Kaiser-windowed time responses in figure 11 are displayed in figure 12. Except for the values near the interface itself, the degradation due to the Gibbs oscillations has been removed. For $z > 50$ m, the reconstructed estimate for $n(z)$ is slightly in error.

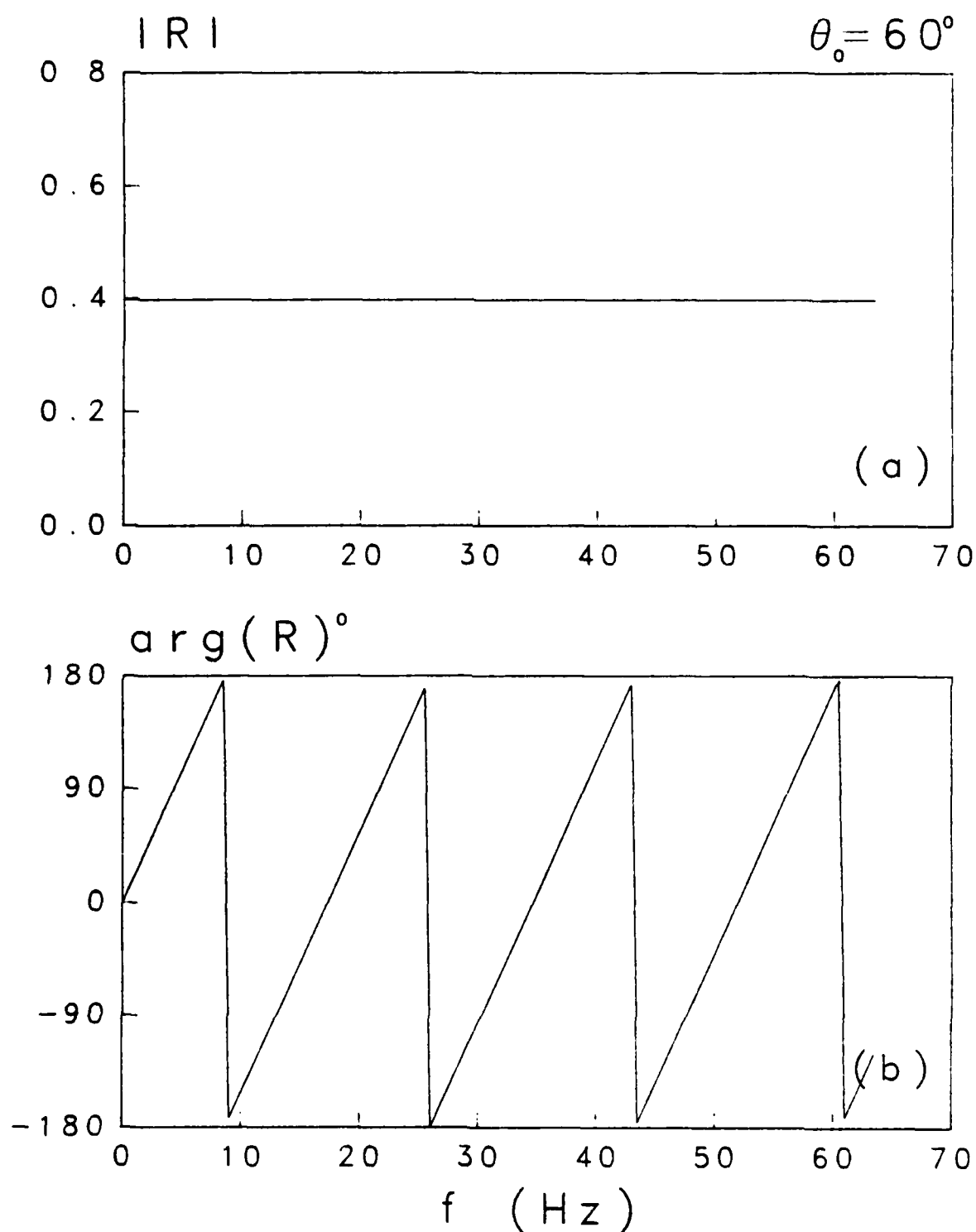


Figure 7. (a) Amplitude and (b) Phase of the Passband Frequency Response of the Reflection Coefficient for Model 2, Grazing Angle $\theta_0 = 60^\circ$.

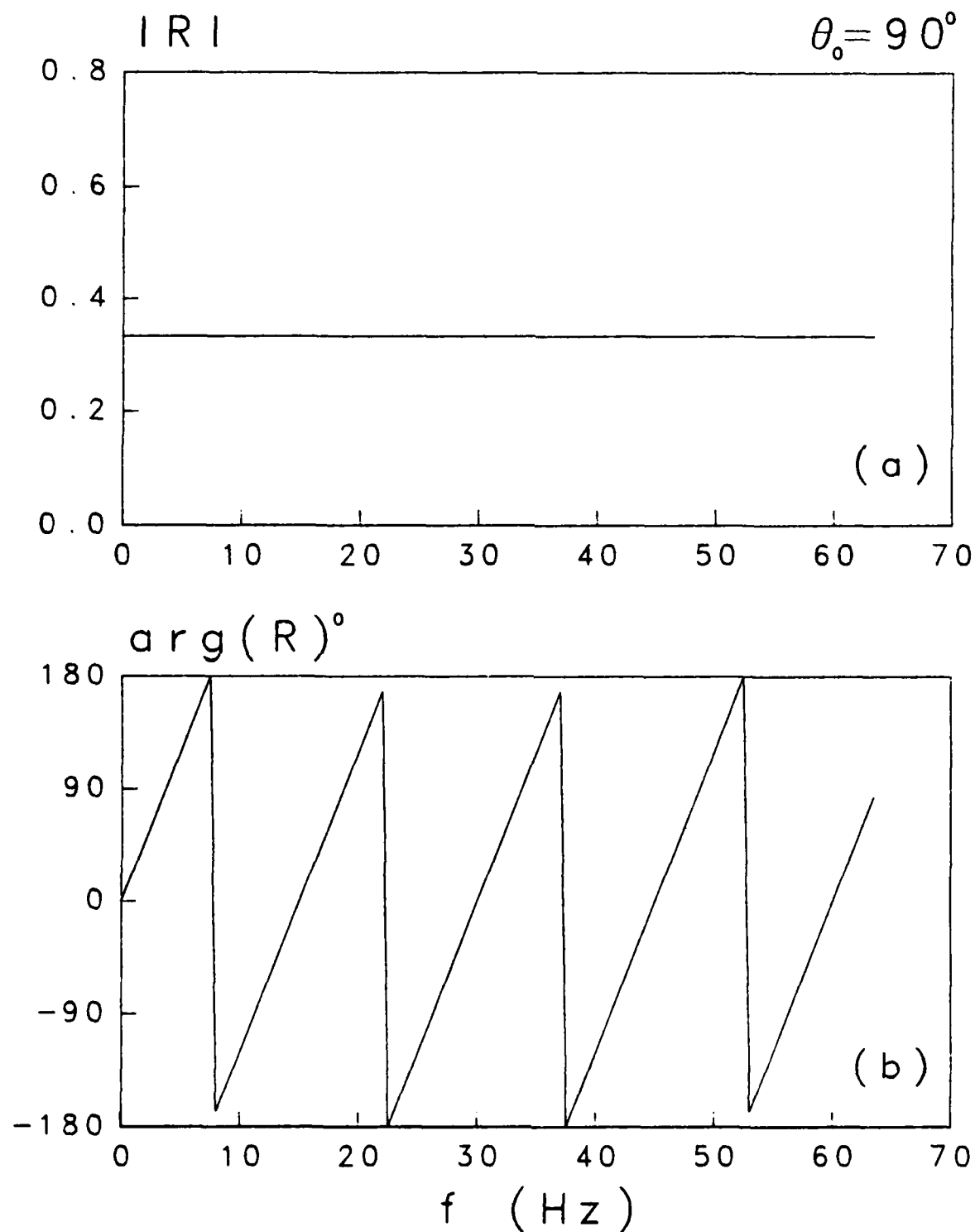


Figure 8. (a) Amplitude and (b) Phase of the Passband Frequency Response of the Reflection Coefficient for Model 2, Grazing Angle $\theta_0 = 90^\circ$

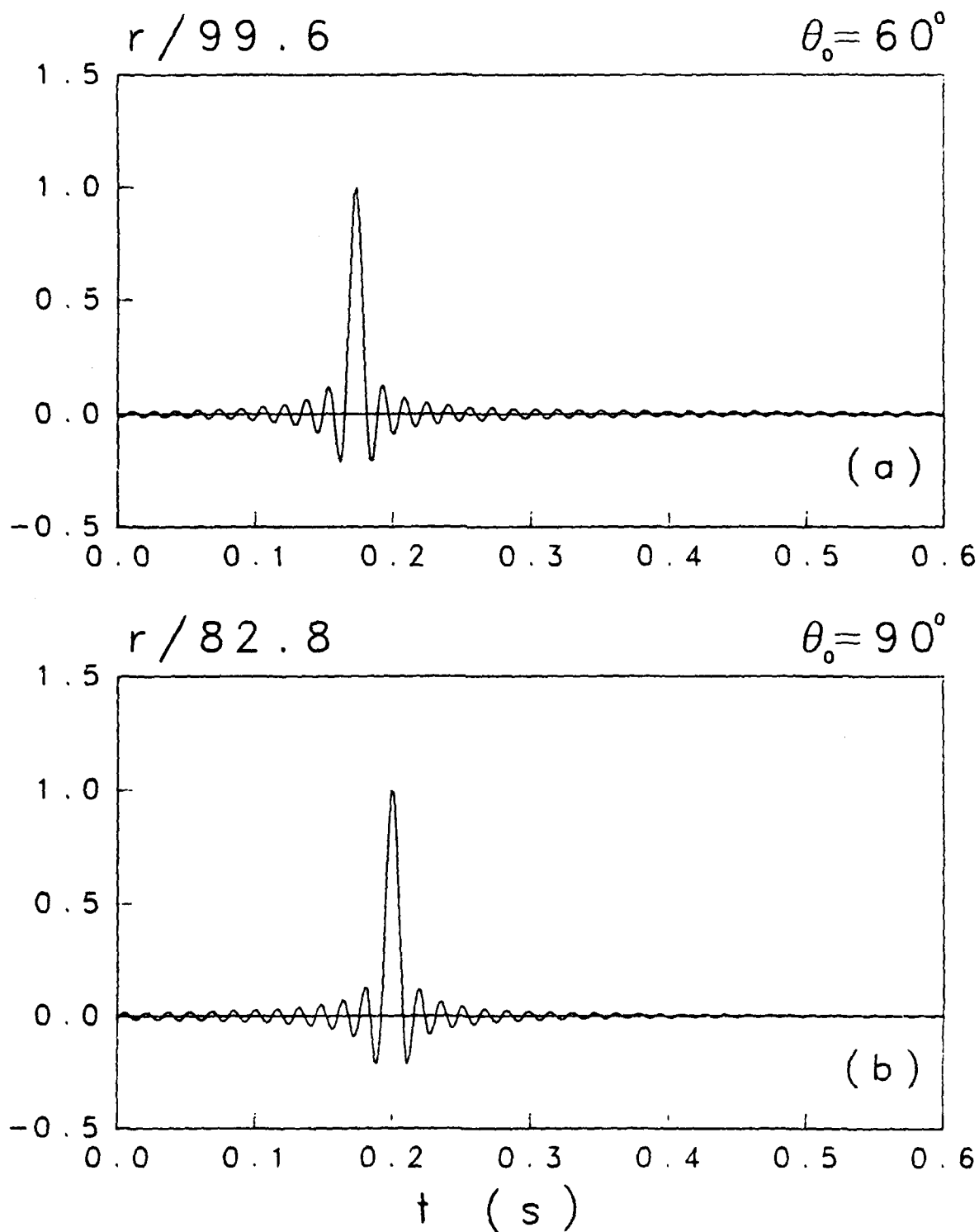


Figure 9. Bandlimited (0-64 Hz) Time Responses of the Reflection Coefficients for Model 2 at Grazing Angles (a) $\theta_0 = 60^\circ$ and (b) $\theta_0 = 90^\circ$, Rectangular Window Filter

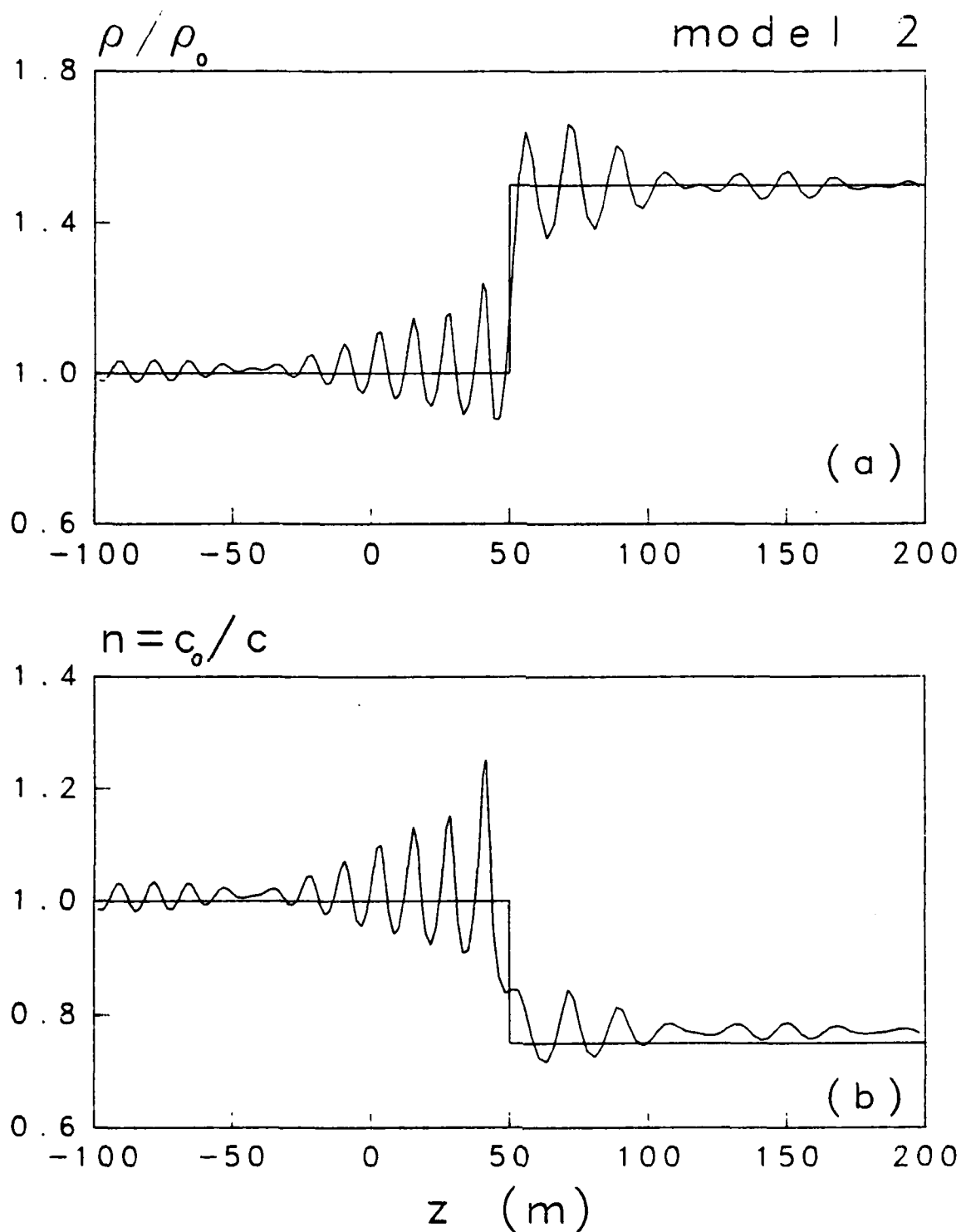


Figure 10. Reconstructed Profiles for Model 2 Using the Time Responses in Figure 9 Showing (a) Normalized Density and (b) Refractive Index

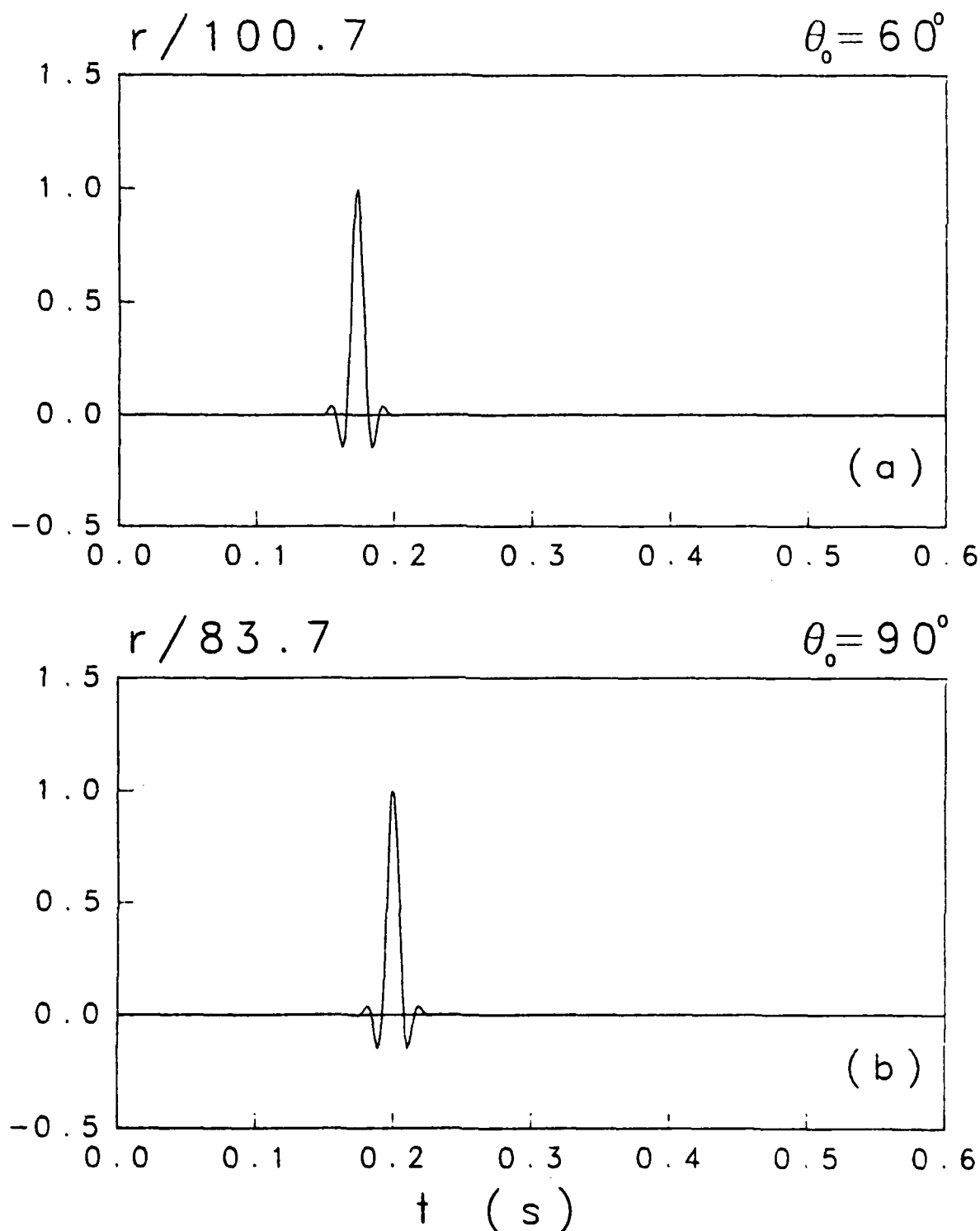


Figure 11. Bandlimited (0-64 Hz) Time Responses of the Reflection Coefficients for Model 2 at Grazing Angles (a) $\theta_0 = 60^\circ$ and (b) $\theta_0 = 90^\circ$, Kaiser Window Filter

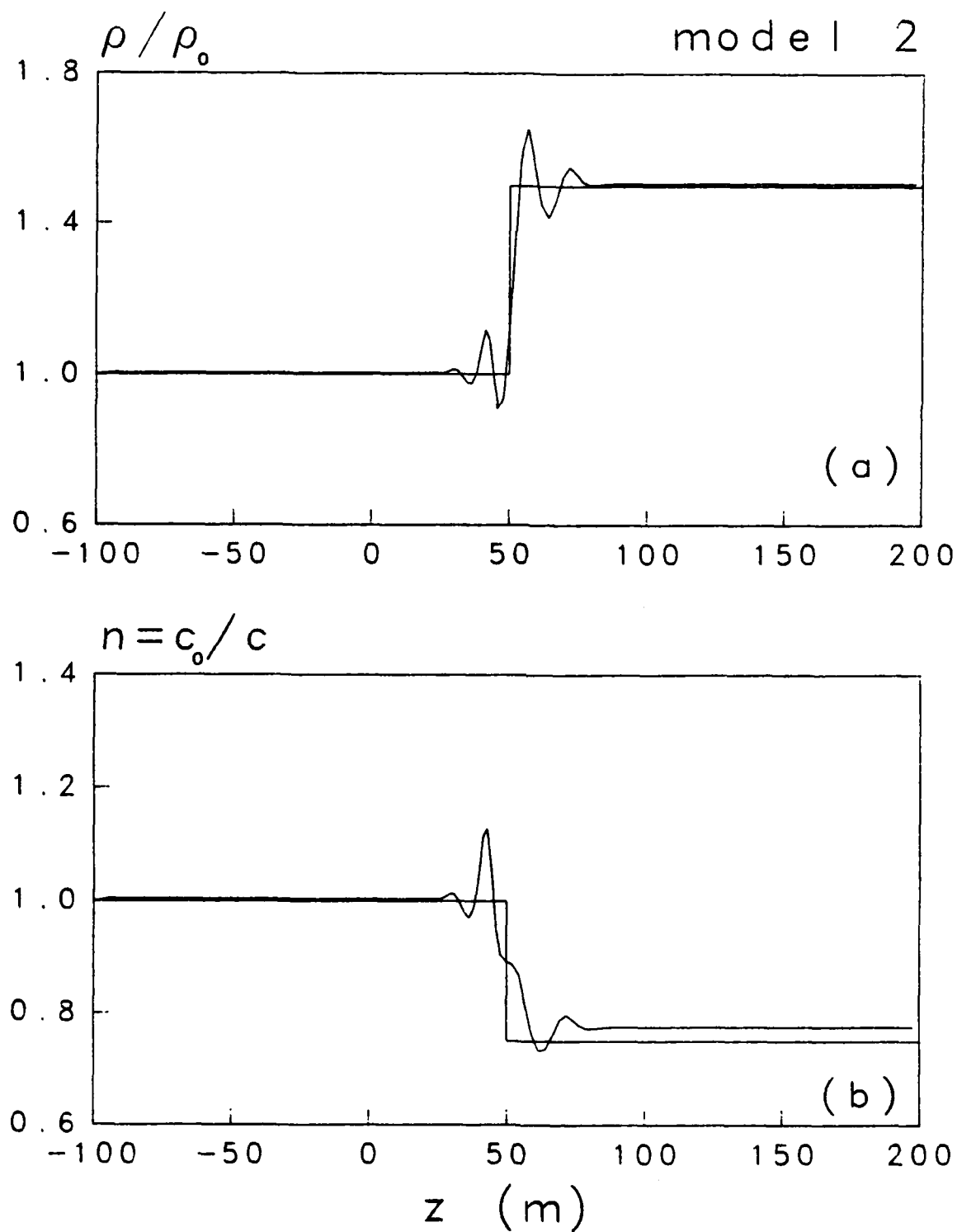


Figure 12. Reconstructed Profiles for Model 2 Using the Time Responses in Figure 11 Showing (a) Normalized Density and (b) Refractive Index

6.3 MODEL 3

The final example is based on a realistic geoacoustic model for the Hatteras Abyssal Plain region. This model was deduced from seismic analysis of time waveforms measured at many source-receiver ranges. The reconstruction below is based on impulse responses for two distinct grazing angles corresponding to only two source-receiver offsets. The frequency responses computed for this model are shown in figure 13 for $\theta_0 = 60^\circ$ and in figure 14 for $\theta_0 = 90^\circ$. In these responses the modulations are indicative of multiple reflections. The nonlinear phases result from the sound speed gradients within the thick layer. At the higher frequencies the large values of $|R|$ suggest the presence of discontinuities within the inhomogeneous region.

Figure 15 shows the time responses for this model when a rectangular window filter is used. The three "pulses" observed at both grazing angles correspond to reflections from discontinuities at $z = 0, 20.4$, and 300 m. Between the second and third reflections, continuous returns are observed from the deep layer. The Gibbs oscillations are pronounced. The reconstructed values of $\rho(z)$ and $n(z)$ based on the time series in figure 15 are given in figure 16 together with the model values. In spite of the Gibbs oscillations, the global behavior of the reconstructions agree well with the model inputs. Although the density jump within the thin layer is indicated, the sound speed change is not readily apparent at that depth. For the highest frequency allowed in the bandlimited time responses, the thin layer is less than one wavelength thick. Higher frequencies are required to obtain better resolution in depth.

The time responses obtained using the same Kaiser window filter described earlier are presented in figure 17. Now the continuous reflections from the thick layer are more easily observed. With these time responses used in the inversion algorithm, the reconstructed results shown in figure 18 are obtained. Except for the poor resolution of $n(z)$ near the thin upper layer, the reconstructions agree well with the model inputs, particularly for the density values. The value of $c_0/c(z)$ for $z > 300$ m is slightly in error.

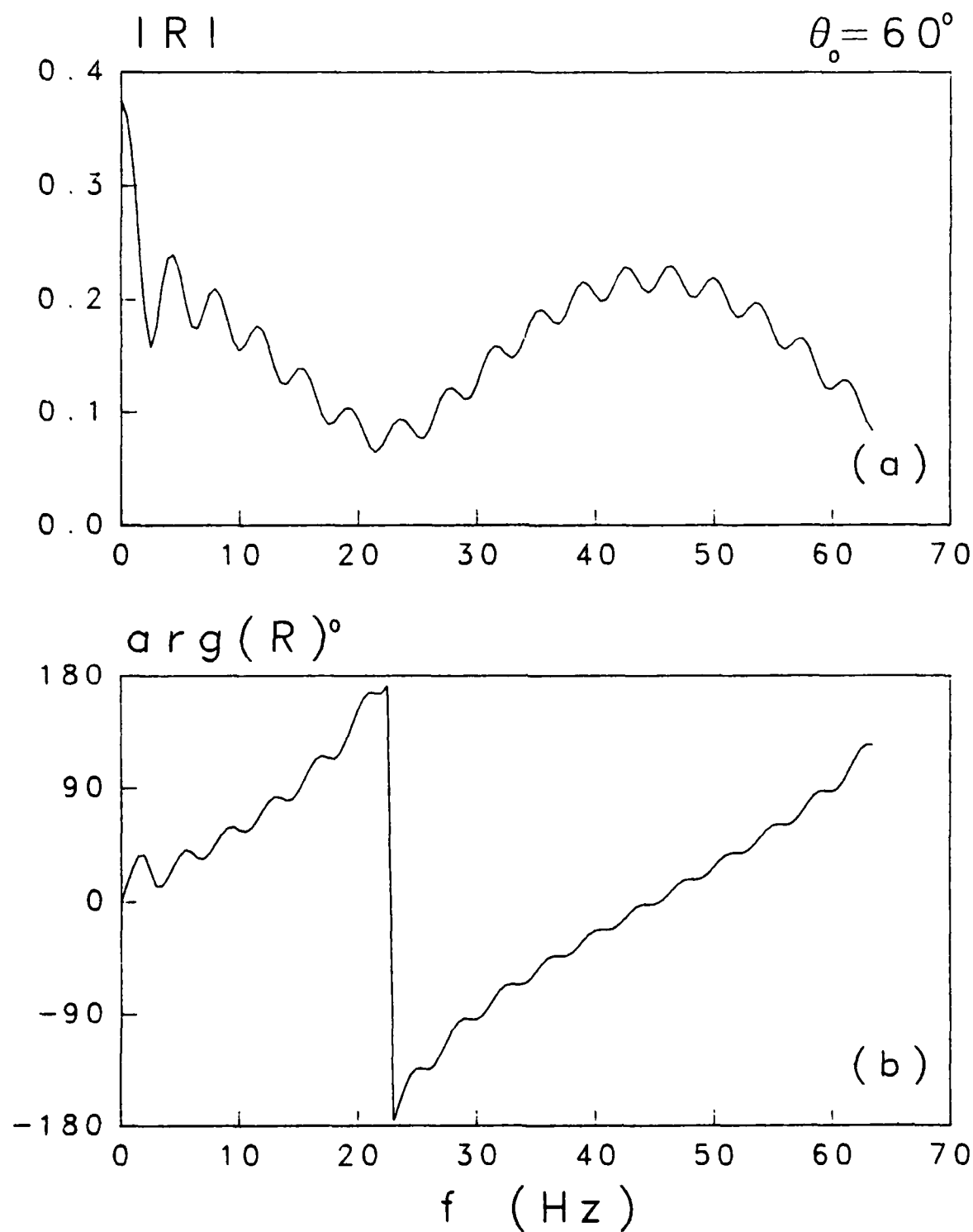


Figure 13. (a) Amplitude and (b) Phase of the Passband Frequency Response of the Reflection Coefficient for Model 3, Grazing Angle $\theta_0 = 60^\circ$

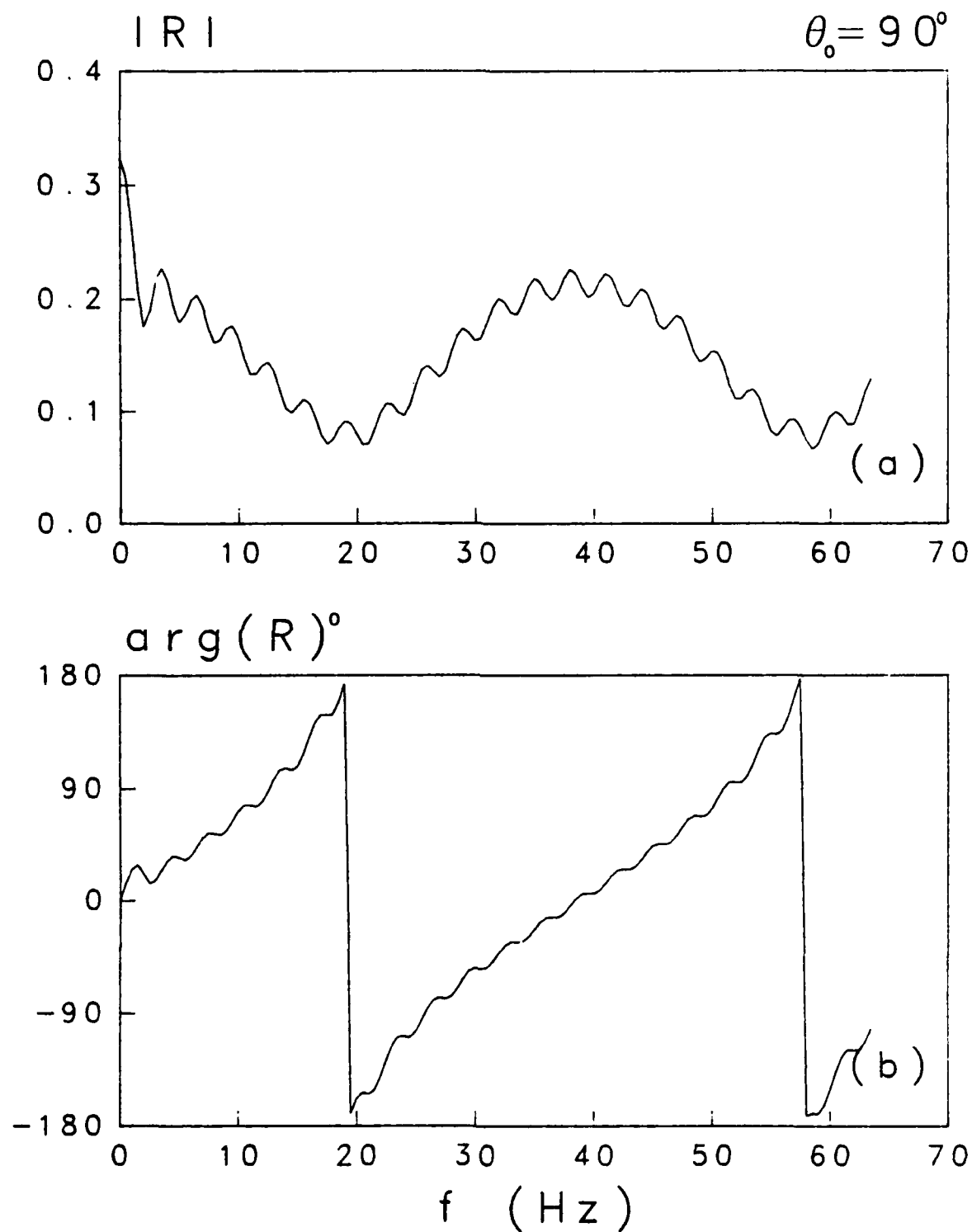


Figure 14. (a) Amplitude and (b) Phase of the Passband Frequency Response of the Reflection Coefficient for Model 3, Grazing Angle $\theta_0 = 90^\circ$

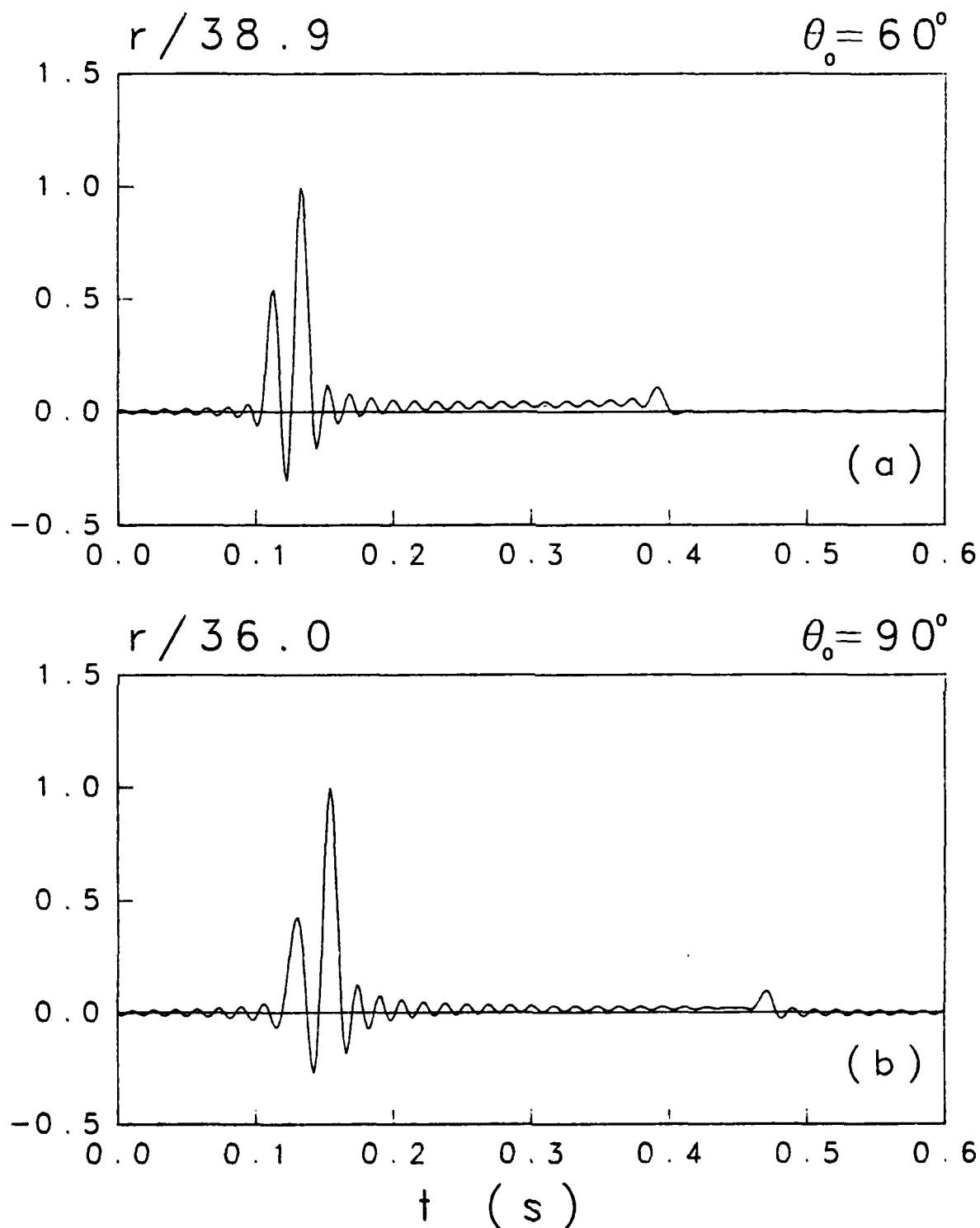


Figure 15. Bandlimited (0-64 Hz) Time Responses of the Reflection Coefficients for Model 3 at Grazing Angles (a) $\theta_0 = 60^\circ$ and (b) $\theta_0 = 90^\circ$, Rectangular Window Filter

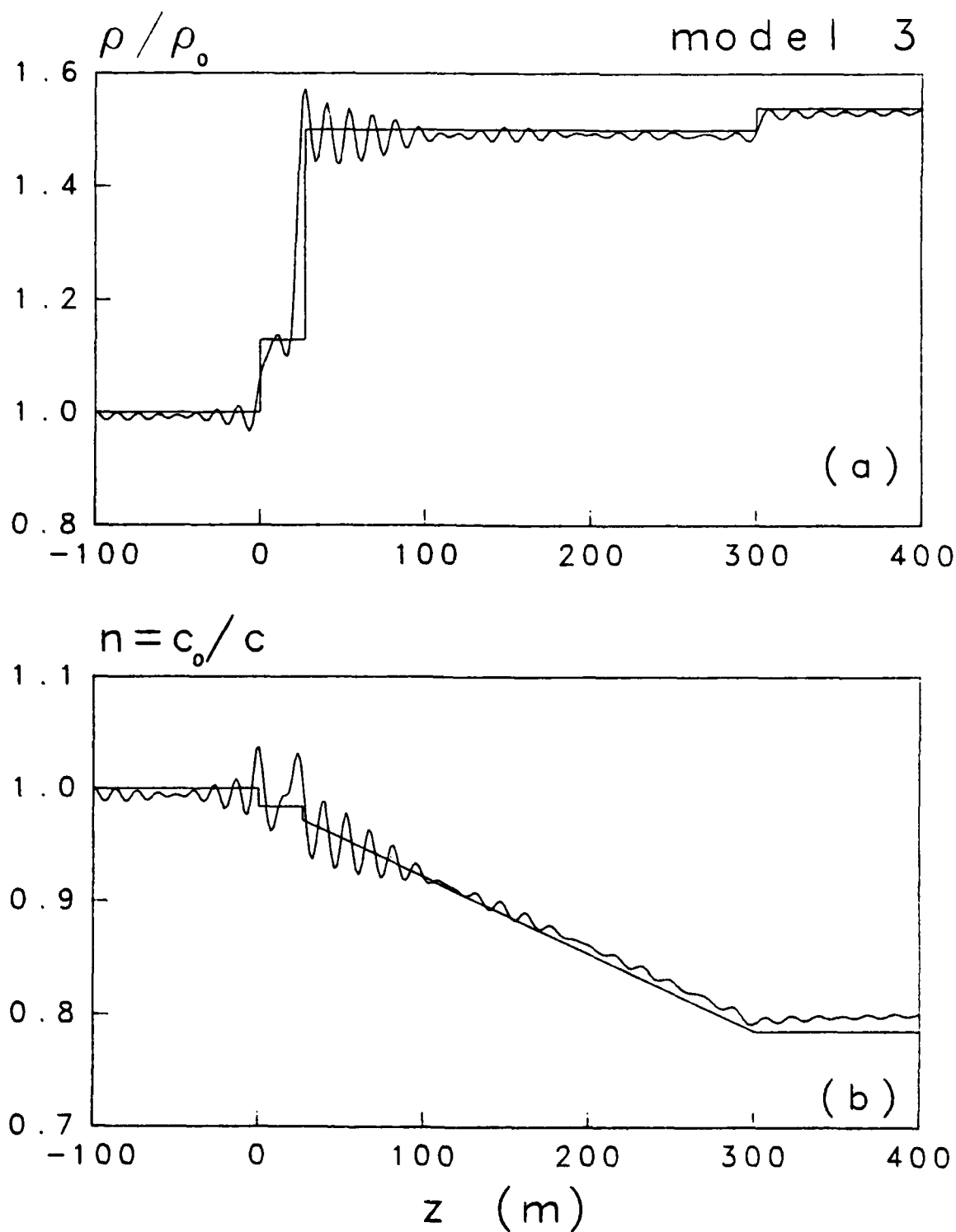


Figure 16. Reconstructed Profiles for Model 3 Using the Time Responses in Figure 15 Showing (a) Normalized Density and (b) Refractive Index

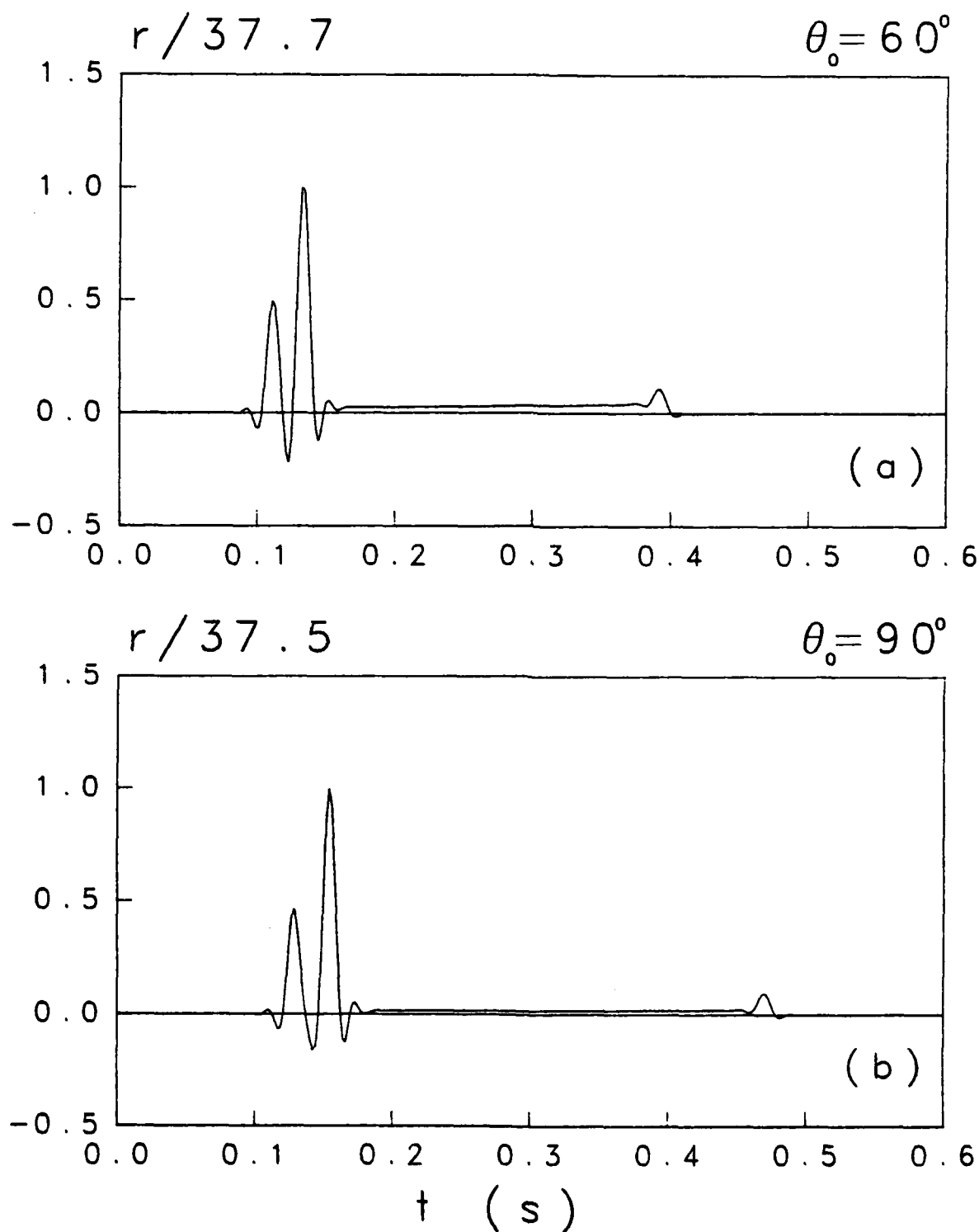


Figure 17. Bandlimited (0-64 Hz) Time Responses of the Reflection Coefficients for Model 3 at Grazing Angles (a) $\theta_0 = 60^\circ$ and (b) $\theta_0 = 90^\circ$, Kaiser Window Filter

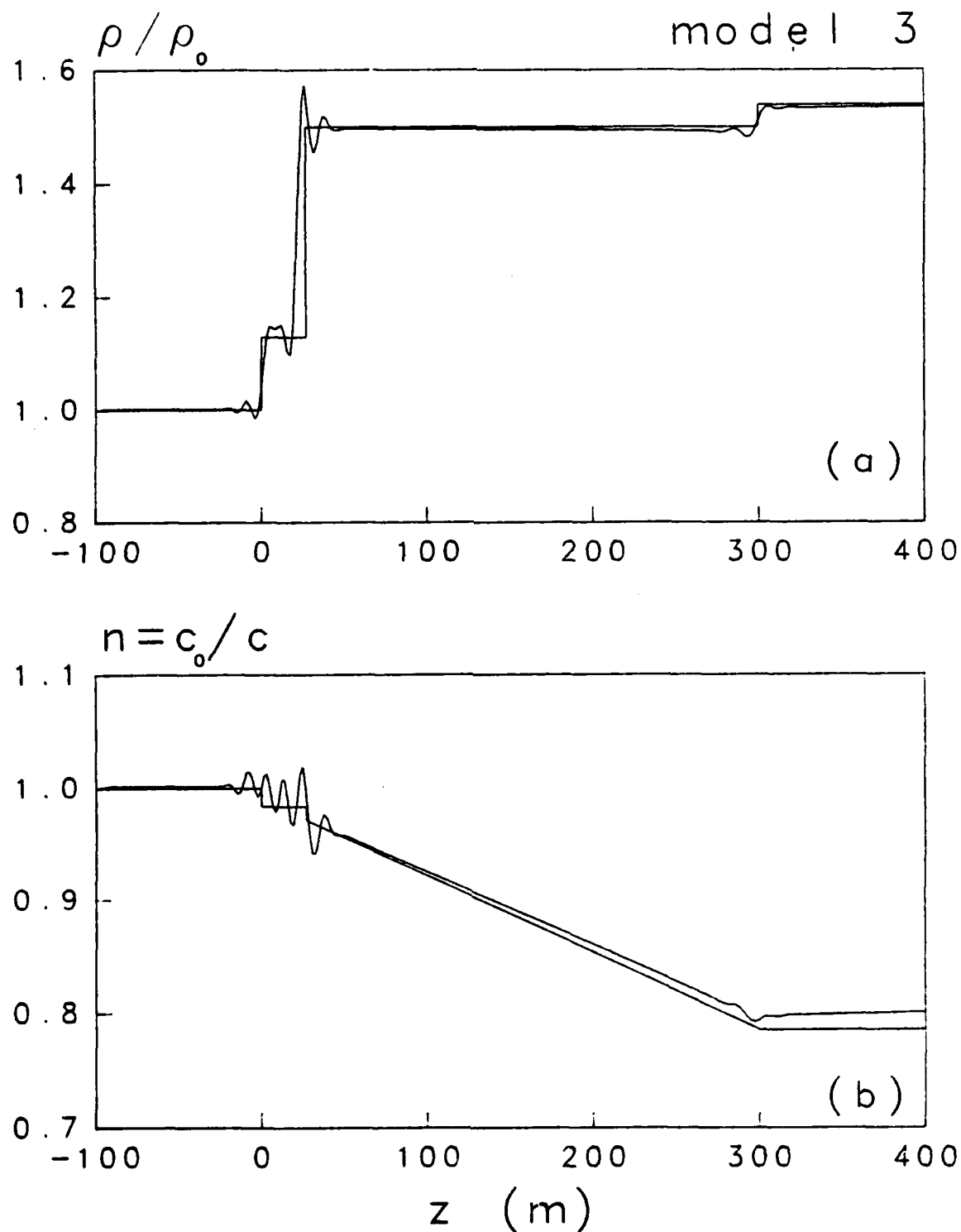


Figure 18. Reconstructed Profiles for Model 3 Using the Time Responses in Figure 17 Showing (a) Normalized Density and (b) Refractive Index

7. SUMMARY

The inversion method of Candel et al.^{4,5} has been implemented with a view to recovering the acoustic properties of a layered ocean bottom. For the scattering of acoustic plane waves, the method permits the reconstruction of both the density and the sound speed profiles via numerical integration of a system of four first-order differential equations. Reflection data for two distinct grazing angles are required. To test the code, noise-free reflection data in the form of bandlimited impulse responses were generated synthetically for three nonabsorbing inhomogeneous models. The results of the numerical inversions are in good agreement with the original models. However, the effects of absorption and noisy reflection data require further investigation.

8. REFERENCES

1. S. R. Santaniello, F. R. DiNapoli, R. K. Dullea, and P. D. Herstein, "Studies on the Interaction of Low-Frequency Acoustic Signals With the Ocean Bottom," Geophysics, 44, 1979, pp. 1922-1940.
2. R. Burridge, "The Gelfand-Levitan, the Marchenko, and the Gopinath-Sondhi Integral Equations of Inverse Scattering Theory, Regarded in the Context of Inverse Impulse-Response Problems," Wave Motion, 2, 1980, pp. 305-323.
3. R. G. Newton, "Inversion of Reflection Data for Layered Media: A Review of Exact Methods," Geophys. J. R. Astr. Soc., 65, 1981, pp. 191-215.
4. S. M. Candel, F. Defillipi, and A. Launay, "Determination of the Inhomogeneous Structure of a Medium From Its Plane Wave Reflection Response, Part I: A Numerical Analysis of the Direct Problem," J. Sound Vib., 68, 1980, pp. 571-582.
5. S. M. Candel, F. Defillipi, and A. Launay, "Determination of the Inhomogeneous Structure of a Medium From Its Plane Wave Reflection Response, Part II: A Numerical Approximation," J. Sound Vib., 68, 1980, pp. 583-595.
6. J. F. Claerbout, Fundamentals of Geophysical Data Processing, McGraw-Hill Book Company, Inc., NY, 1976.
7. R. W. Clayton and R. H. Stolt, "A Born-WKB Inversion Method for Acoustic Reflection Data," Geophysics, 46, 1981, pp. 1559-1567.
8. S. H. Gray and F. Hagin, "Toward Precise Solution of One-Dimensional Velocity Inverse Problems," SIAM J. Appl. Math., 42, 1982, pp. 346-355.
9. S. H. Gray, "A Geometrical-Optical Series and a WKB Paradox," Quart. Appl. Math., 40, 1982, pp. 73-81.
10. C. Q. Lee, "Wave Propagation and Profile Inversion in Lossy Inhomogeneous Media," Proc. IEEE, 70, 1982, pp. 219-228.
11. F. Santosa, "Numerical Scheme for the Inversion of Acoustical Impedance Profile Based on the Gelfand-Levitan Method," Geophys. J. R. Astr. Soc., 70, 1982, pp. 229-244.
12. F. Santosa and H. Schwetlick, "The Inversion of Acoustical Impedance Profile by Methods of Characteristics," Wave Motion, 4, 1982, pp. 99-110.
13. L. M. Brekhovskikh, Waves in Layered Media, Academic Press, NY, 1960.
14. S. A. Schelkunoff, "Remarks Concerning Wave Propagation in Stratified Media," Commun. Pure Appl. Math., 4, 1951, pp. 117-128.
15. F. W. Sluijter, "Arbitrariness of Dividing the Total Field in an Optically Inhomogeneous Medium Into Direct and Reversed Waves," J. Opt. Soc. Am., 60, 1970, pp. 8-10.

16. L. C. Baird, "New Integral Formulation of the Schrodinger Equation," J. Math. Phys., 11, 1970, pp. 2235-2242.
17. F. D. Tappert, "The Parabolic Approximation Method," in Wave Propagation and Underwater Acoustics, eds. J. B. Keller and J. S. Papadakis, Springer-Verlag Inc., NY, 1977.
18. J. M. McKisic and D. P. Hamm, "New Method for Normal-Mode Models of Sound Propagation in the Ocean," J. Acoust. Soc. Am., 59, 1976, pp. 294-304.
19. N. R. Chapman and R. S. Sloboda. "The Plane Wave Reflection Coefficient for a Three-Layer Model of the Ocean Bottom, Defence Research Establishment Pacific (DREP), Technical Memorandum 81-8, 1981.
20. L. F. Shampine and M. K. Gordon, Computer Solution of Ordinary Differential Equations, W. H. Freeman and Co., San Francisco, CA, 1975.
21. N. R. Chapman and B. Huber, "Numerical Calculation of the Plane Wave Reflection Coefficient for Realistic Geoacoustic Bottom Models, Defence Research Establishment Pacific (DREP), Technical Memorandum 81-10, 1981.
22. F. R. DiNapoli, D. Potter, and P. Herstein, "Comparison of Synthetic and Experimental Bottom Interactive Waveforms," in Bottom-Interacting Acoustics, eds W. A. Kuperman and F. Jensen, Plenum Press, NY, 1980, pp. 225-237.
23. E. O. Brigham, The Fast Fourier Transform, Prentice-Hall, Inc., Englewood Cliffs, NJ, 1976.
24. G. D. Bergland and M. T. Dolan, "Fast Fourier Transform Algorithms," in Programs for Digital Signal Processing, IEEE Press, NY, 1979.
25. L. R. Rabiner, C. A. McGonegal, and D. Paul, "FIR Windowed Filter Design Program - WINDOW," in Programs for Digital Signal Processing, IEEE Press, NY, 1979.

Appendix

RICATTI EQUATION FOR U/D

While the local fields U and D satisfy the coupled system in equation (20), the reflection coefficient $R = U/D$ satisfies a nonlinear differential equation. It is straightforward to show that

$$R' = (U/D)' = U'/D - UD'/D^2 = -2ik_z R + g(1 - R^2), \quad (A-1)$$

where U' and D' were eliminated via the system in equation (20). Equation (A-1) is of the Ricatti type. From initial conditions (22) and (23), it follows that

$$R(H) = 0. \quad (A-2)$$

Recalling the jump conditions (28) and (29) on the U and D fields at discontinuities in the medium, it can be shown that the ratio U/D undergoes a jump condition given by

$$R_- = [(1 - Y_+/Y_-) + (1 + Y_+/Y_-)R_+][(1 + Y_+/Y_-) + (1 - Y_+/Y_-)R_+]^{-1}. \quad (A-3)$$

This Ricatti equation is readily converted into the integral form,

$$R(z) = \int_H^z g(s) [1 - R(s)^2] \exp \left[2i \int_z^s k_z(t) dt \right] ds, \quad (A-4)$$

where the limits of integration were adjusted in the same way as that which preceded equation (37).

The success of the approximation given in equation (37) appears to rely on $|B| \ll |A|$. This suggests that equation (A-4) can be solved by iteration whenever U/D is small. In the zeroth approximation, we substitute $R^{(0)} = 0$ into the integrand of equation (A-4) to obtain for the next iterate, when evaluated at $z = 0$, the result,

$$R^{(1)}(0) = - \int_0^H g(s) \exp \left[2i \int_0^s k_z(t) dt \right] ds, \quad (A-5)$$

which is in agreement with equations (37) and (47).

INITIAL DISTRIBUTION LIST

Addressee	No. of Copies
ASN (RE&S)	1
OUSDR&E (Research and Advanced Technology)	1
Principal Dep Assist Secretary (Research)	1
DARPA (TTO)	1
DARPA (CDR K. Evans)	1
CNO (OP-095; -96; -098; CAPT E. Young, CDR H. Dantzler, 9520)	5
CNM (SPO PM-2; MAT-052; -0723; CAPT J. Harlett, -0724; R. Hillyer, -05; L. L. Hill, -907)	6
NAVELECSYSCOM (R. Mitnick, J. Schuster, ELEX 612; R. Knudsen, PME-124)	3
NAVSEASYSYSCOM (SEA-63; -63D; -63D3; D. Porter, F. Romano, R. Farwell, -63R; -63-R-1; -63R-13)	8
NAVPGSCOL	1
DWTNSRDC	1
NORDA (Code 105; 320; R. Lauer, 320; S. Marshall, 115; R. Martin, 110A; E. Chiaka, B. Blumenthal, W. Worsley, R. Wheatly, 530; J. Matthews; G. Stanford; Library)	12
NOSC (M. Pederson, D. Gordon, 712; J. R. McCarthy, 713; C. Persons, 7133; S. Sullivan, 1604; R. Smith; J. Lovett; G. Tunstall; Library)	9
NADC (J. Howard; B. Steinberg; P. Haas; Library)	4
NCSC	1
NSWC (R. Stevenson; M. Stripling; M. Stallard; Library)	4
NRL (O. Diachok, R. Dicus, 5160; M. Munson, 5100; W. Mosley, 5120; A. Eller, 5109; Library)	6
MPL (V. C. Anderson; F. Fischer; B. Williams)	3
NAVAIR (E. David, 370B; W. Parrigian, 370J)	2
NISC (H. Foxwell)	1
DTIC	2
ONR (ONR-102; R. Winokur, -102B; -200; CAPT E. Craig, T. Warfield, -220; G. Hamilton, -420; -422; -425AC; J. McKisic, -4250A; P. Rogers, -425UA; J. A. Smith; -100; -480)	13
DIA	1
CHESNAVFACENGCOM	1
ARL (Univ. of Texas) (P. Vidmar; K. Hawker; R. Koch; Library)	4
ARL (Penn State Univ.) (S. McDaniel; Dr. McCammon; Library)	3
Courant Institute (D. C. Stickler; Library)	2
SAI (C. W. Spofford, R. Greene)	2
Cornell University (H. Schwetlick)	1
Northwestern University (G. Kriegsmann)	1
Univ. of Denver (J. A. DeSanto; F. Hagin)	2
Univ. of Miami (F. Tappert)	1
General Instrument Co. (R. Breton)	1
FWG (P. Wille)	1
Woods Hole Oceanographic Institution	1
Marine Physical Lab, Scripps	1

INITIAL DISTRIBUTION LIST (Cont'd)

Addressee	No. of Copies
CANADA	
DREP	20
DSIS (Microfiche Section, Report Collection)	3
DREA	1
ORAE Library (DMOR)	2
CDLS/L CDR	1
CDLS/W CDR	1
CMDO	1
DMRS	1
Commander Maritime Command (MC/ORD, SSO Ocean)	2
CFMWS	1
Maritime Hdqrs. Pacific (SSO Op Rsch)	1
DST (SE)3	1
DTA (M)3	1
RRMC (Dept. of Oceanography)	1
D Met Oc	1
Project Officer IEP ABCANZ-2, NOP 981, Pentagon	3
BRITAIN	
DRIC	3
AUWE	1
RAE	1
AUSTRALIA	
DRC	1
NEW ZEALAND	
DSE	1

END

FILMED

10-83

DTIC